EARTH SURFACE PROCESSES AND LANDFORMS
Earth Surf. Process. Landforms **43**, 1133–1154 (2018)

Published online 14 February 2018 in Wiley Online Library
(wileyonlinelibrary.com) DOI: 10.1002/esp.4306

Which way do you lean? Using slope aspect variations to understand Critical Zone processes and feedbacks

Jon D. Pelletier,[1]* Greg A. Barron-Gafford,[2] Hugo Gutiérrez-Jurado,[3] Eve-Lyn S. Hinckley,[4] Erkan Istanbulluoglu,[5] Luke A. McGuire,[1] Guo-Yue Niu,[6] Michael J. Poulos,[7] Craig Rasmussen,[8] Paul Richardson,[9] Tyson L. Swetnam[10] and Greg E. Tucker[11]

[1] Department of Geosciences, The University of Arizona, Tucson, Arizona USA
[2] School of Geography and Development, The University of Arizona, Tucson, Arizona USA
[3] Department of Geological Sciences, The University of Texas at El Paso, El Paso, Texas USA
[4] Institute of Arctic and Alpine Research and Environmental Studies Program, University of Colorado, Boulder, Colorado USA
[5] Department of Civil and Environmental Engineering, University of Washington, Washington, USA
[6] Department of Hydrology and Atmospheric Sciences, The University of Arizona, Tucson, Arizona USA
[7] Department of Geosciences, Boise State University, Boise, Idaho USA
[8] Department of Soil, Water, and Environmental Sciences, University of Arizona, Tucson, Arizona USA
[9] Department of Earth Sciences, 1272 University of Oregon, Eugene, Oregon USA
[10] BIO5 Institute, The University of Arizona, Tucson, Arizona USA
[11] Cooperative Institute for Research in Environmental Sciences (CIRES) and Department of Geological Sciences, 2200 Colorado Ave, University of Colorado, Boulder, Colorado USA

Received 22 March 2017; Revised 21 November 2017; Accepted 23 November 2017

*Correspondence to: Jon D. Pelletier, Department of Geosciences, The University of Arizona, Gould-Simpson Building, 1040 East Fourth Street, Tucson, Arizona 85721-0077, USA. E-mail: jdpellet@email.arizona.edu

ESPL
Earth Surface Processes and Landforms

ABSTRACT: Soil-mantled pole-facing hillslopes on Earth tend to be steeper, wetter, and have more vegetation cover compared with adjacent equator-facing hillslopes. These and other slope aspect controls are often the consequence of feedbacks among hydrologic, ecologic, pedogenic, and geomorphic processes triggered by spatial variations in mean annual insolation. In this paper we review the state of knowledge on slope aspect controls of Critical Zone (CZ) processes using the latitudinal and elevational dependence of topographic asymmetry as a motivating observation. At relatively low latitudes and elevations, pole-facing hillslopes tend to be steeper. At higher latitudes and elevations this pattern reverses. We reproduce this pattern using an empirical model based on parsimonious functions of latitude, an aridity index, mean-annual temperature, and slope gradient. Using this empirical model and the literature as guides, we present a conceptual model for the slope-aspect-driven CZ feedbacks that generate asymmetry in water-limited and temperature-limited end-member cases. In this conceptual model the dominant factor driving slope aspect differences at relatively low latitudes and elevations is the difference in mean-annual soil moisture. The dominant factor at higher latitudes and elevations is temperature limitation on vegetation growth. In water-limited cases, we propose that higher mean-annual soil moisture on pole-facing hillslopes drives higher soil production rates, higher water storage potential, more vegetation cover, faster dust deposition, and lower erosional efficiency in a positive feedback. At higher latitudes and elevations, pole-facing hillslopes tend to have less vegetation cover, greater erosional efficiency, and gentler slopes, thus reversing the pattern of asymmetry found at lower latitudes and elevations. Our conceptual model emphasizes the linkages among short- and long-timescale processes and across CZ sub-disciplines; it also points to opportunities to further understand how CZ processes interact. We also demonstrate the importance of paleoclimatic conditions and non-climatic factors in influencing slope aspect variations. Copyright © 2017 John Wiley & Sons, Ltd.

KEYWORDS: insolation; slope aspect; hillslope asymmetry; feedbacks; Critical Zone

Problem statement

What is slope aspect and why is it important?

The development of Critical Zone (CZ) science is motivated by the fact that landscape development is controlled by feedbacks among hydrologic, ecologic, pedogenic, and geomorphic processes operating over a wide range of timescales from individual weather events to millions of years. The study of landscape or CZ development is challenging, in part, because each landscape has its own unique combination of lithology, tectonic uplift rate, and climate. Investigating the slope aspect control on CZ stocks and fluxes is a potentially powerful means of understanding CZ development because insolation is often the primary difference between adjacent pole- and equator-facing hillslopes. There, lithology, tectonic uplift rate, and

climate can sometimes be approximated as uniform, leaving microclimatic differences related to insolation as the dominant driver of differences in CZ development between hillslopes of opposing aspect. Insolation exerts a direct control on ground surface temperatures and potential evapotranspiration rates. From these primary microclimatic drivers, differences in many CZ state variables can emerge over time. The overarching questions of this paper are: (1) what processes and feedbacks are occurring at places where aspect dependence is apparent? and (2) what can they tell us about CZ development?

The primary goal of this paper is to use slope aspect as a means of identifying common feedbacks among CZ processes, with a particular emphasis on linking short- and long-timescale processes. We aim to provide a global perspective on the slope aspect control of CZ processes. The variety of results that have been reported in the literature regarding slope aspect control on CZ processes can suggest that no unifying set of results or conceptual model exists. We aim to demonstrate that many slope aspect studies of soil-mantled landscapes can be usefully synthesized by considering water-limited and temperature-limited cases as end members.

The roadmap of this paper is as follows. First, we present continental-scale patterns in the slope aspect control of topographic asymmetry of hillslopes, results that are based primarily on the methods of Poulos et al. (2012). Second, we introduce a novel empirical model that reproduces these patterns based on latitude, an aridity index, mean-annual temperature, and mean slope gradient. This model serves as a discussion point and unifying theme for the remainder of the paper. Our proposed model suggests that the aspect control of hillslopes can be considered as a continuum between a water-limited end member in which the lower potential evaporation of pole-facing hillslopes drives higher mean soil moisture, triggering feedbacks that result in steeper slopes compared with adjacent equator-facing hillslopes, and a temperature-limited end member in which lower temperatures on pole-facing hillslopes limit vegetation cover and reverse many of the feedbacks associated with the water-limited case. Third, we use the framework of water- and temperature-limited end-member cases to explore the process feedbacks that exist within these cases. Results from the literature that are not consistent with this framework can, in some cases, be understood as a result of cooler climatic conditions (relative to the present interglacial period) that predominated during the Quaternary era, tectonic tilting, and/or structural controls on asymmetry. Finally, we discuss the implications of the slope aspect control of CZ processes for potentially forecasting the response of the CZ to global climate changes that are expected to occur in this century.

Global and regional patterns of topographic asymmetry

We begin our exploration of slope aspect variations of CZ states and fluxes by considering continental-scale patterns of topographic (i.e. slope gradient) asymmetry. This is a useful starting point because topographic asymmetry has been mapped at global scales (Poulos *et al.*, 2012) and because topography develops via the integrated effect of both short-timescale (e.g. runoff vs infiltration) and long-timescale (e.g. soil production) processes. Figure 1 maps hillslope asymmetry, $HA_{N\text{-}S}$, defined

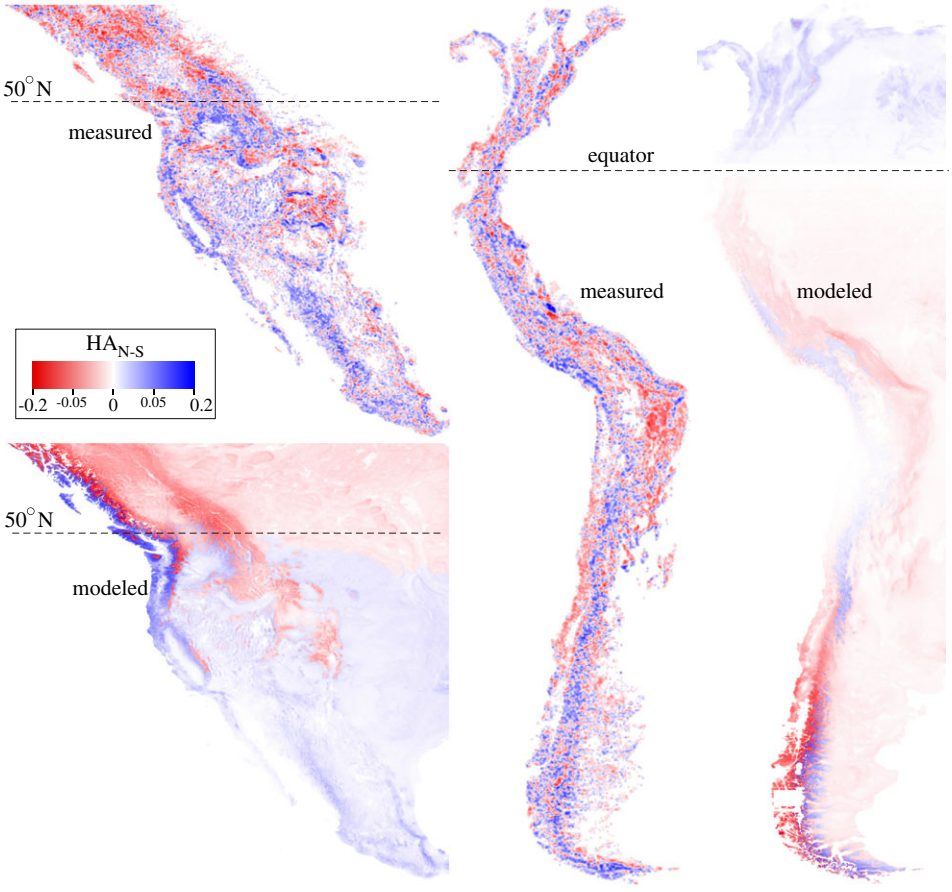

Figure 1. Color maps of measured (Poulos *et al.*, 2012) and modeled (Equation (1)) hillslope asymmetry ($HA_{N\text{-}S}$) for the North and South American Cordillera. Blue colors indicate areas where north-facing hillslopes are steeper, on average, while red values indicate a prevalence of steeper south-facing hillslopes. [Colour figure can be viewed at wileyonlinelibrary.com]

as the log-transformed ratio of the average slope angles of north- and south-facing hillslopes (Poulos *et al.*, 2012). These $HA_{N\text{-}S}$ values were computed using the gap-filled 3 arc-second Shuttle Radar Topography Mission (SRTM) Digital Elevation Models (DEMS) (Jarvis et al., 2008). The resulting $HA_{N\text{-}S}$ values were then averaged to 30 arc-seconds pixel^{-1} to facilitate comparison with the empirical model. Areas with average slope gradients less than 5% are excluded from the analysis (Poulos *et al.*, 2012). Positive values of $HA_{N\text{-}S}$ indicate steeper north-facing hillslopes, on average, while negative values indicate steeper south-facing hillslopes.

Figure 1 documents steeper pole-facing hillslopes throughout most of the western USA. At latitudes higher than approximately 50°N, this pattern reverses (red colors predominate, indicating steeper south-facing hillslopes). Elevation also exerts a significant control on $HA_{N\text{-}S}$ values. In the western USA, elevations above approximately 2 km tend to be exceptions to the general rule of steeper mid-latitude pole-facing hillslopes (i.e. higher elevations tend to be more red than blue in the western USA). South of the equator, low latitudes and elevations also tend to have steeper pole-facing hillslopes (which correspond to negative $HA_{N\text{-}S}$ values). For example, at the widest point of the central Andes, pole- or south-facing hillslopes tend to be steeper (illustrated by the predominantly red colors) in the Andean Eastern Cordillera and Subandes, which are generally less than 3 km in elevation. As with the North American Cordillera, this pattern reverses at high elevations, i.e. blue colors predominate in in the Altiplano-Puna region and the high peaks of the Andean Cordillera Real, which have elevations from 3 to 7 km a.s.l.

Figure 2(a) plots the average $HA_{N\text{-}S}$ as a function of latitude and elevation for the Northern and Southern Cordillera between 60°S and 60°N. The values plotted are the average $HA_{N\text{-}S}$ values for all areas within each latitude and elevation bin. Four plots are presented: one each for elevations in the range of 0–1, 1–2, 2–3, and 3–4 km a.s.l. Gaps in the plots indicate locations where no cases are available. For example, there are few if any mountains with average elevations above 3 km south of 50°S at the scale of this analysis, hence there is a gap in the plot. The lower plots in Figure 2(a) demonstrate that for relatively low elevations and latitudes, pole-facing hillslopes tend to be steeper. That is, at elevations less than approximately 2 km in the Northern Hemisphere, $HA_{N\text{-}S}$ is positive for latitudes less than approximately 50°N. Similarly, at elevations less than 2 km in the Southern Hemisphere, $HA_{N\text{-}S}$ values are predominantly negative for latitudes to the north of approximately 45–50°S. Closer to the poles, this pattern reverses and equator-facing hillslopes tend to become steeper. The latitude at which this reversal occurs depends on elevation, with a shift to higher elevations at a given latitude having an effect similar to a shift towards higher latitudes at the same elevation. In the Northern American Cordillera, for example, the reversal from steeper pole-facing to steeper equator-facing hillslopes occurs at systematically lower latitudes with increasing elevation: 50–55°N for elevations 0–1 km, 45–50°N for elevations 1–2 km, approximately 40°N for elevations 2–3 km, and 35–40°N for elevations 3–4 km. In the South American Cordillera, a broadly consistent trend occurs.

The patterns documented in Figures 1(a) and 2(a) suggest that steeper pole-facing hillslopes represent a default case which can be reversed for sufficiently low temperatures at high latitudes and/or elevations. We propose that in locations where mean-annual temperatures exceed a threshold value, soil moisture and its effects on CZ process rates are the principal drivers of slope aspect control on topographic asymmetry. Below a threshold mean-annual temperature, temperature becomes a significant limiting factor in the growth of many species of plants. In addition, paraglacial processes can become significant.

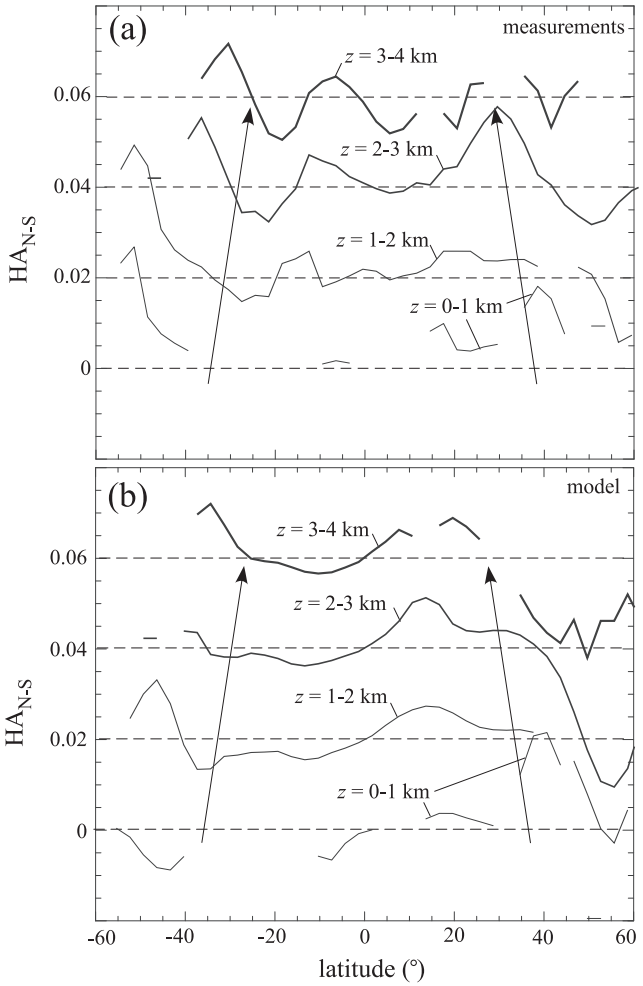

Figure 2. Plots of the topographic asymmetry of hillslopes, $HA_{N\text{-}S}$, for the North and South American Cordillera as a function of latitude and elevation based on (A) measurements and (B) the empirical model of Equation (1). To help differentiate plots, they are shifted up by 0.02 for each 1 km increase in elevation. The arrows help to identify the latitudinal shift in the peak values that occurs with increasing elevation in both the measurements and the model.

Water availability and temperature both strongly control vegetation cover. This suggests a central role for vegetation cover in driving topographic asymmetry at the hillslope scale. Vegetation cover has been invoked as a key variable in influencing topographic asymmetry. In water-limited environments, equator-facing hillslopes have less vegetation cover and hence experience higher erosion rates, since vegetation dissipates flow energy that would otherwise contribute to sediment transport (Melton, 1960; Istanbulluoglu and Bras, 2005; Yetemen et al., 2015a, 2015b; Beudin *et al.*, 2017). In addition, vegetation intercepts raindrops, which increases water lost by evaporation and sublimation (Pomeroy et al., 1998; Marin *et al.*, 2000), and reduces sediment mobilization by raindrop impacts (Dunne *et al.*, 2010). Acosta *et al.* (2015) documented an inverse relationship between vegetation cover and erosion rates across a wide range of slope gradients using cosmogenic nuclides in east Africa.

The development of topographic asymmetry by water limitations has most often been invoked in relatively arid landscapes. However, it is important to note that water limitations on vegetation growth exist even in many relatively humid climates. For example, even in the humid Appalachians, northeast-facing hillslopes tend to have more vegetation cover than southwest-facing hillslopes (Hutchins, 1976). There is growing evidence under a wide range of climates that hillslope diffusivity (which

quantifies the efficiency of sediment transport) increases with mean-annual precipitation (Hanks, 2000; Hurst *et al.*, 2013; Richardson, 2015) such that hillslope diffusivities tend to be largest in humid forested ecosystems that undergo more bioturbation than semiarid grass and shrub dominated ecosystems (Martin, 2000; Gabet and Dunne, 2003; Roering, 2004; Hughes *et al.*, 2009). Besides regional climate, field studies have revealed aspect-modulated micro-climate controls on hillslope diffusion (West *et al.*, 2014) and topographic attributes related to bedrock weathering rates (Burnett *et al.*, 2008; Pelletier and Swetnam, 2017). For example, West *et al.* (2014) found hillslope diffusivities on south-facing hillslopes to be twice as large as those of north-facing hillslopes in a forested watershed in central Pennsylvania, USA.

Figures 1 and 2 also present the results of an empirical model that predicts the broad-scale global patterns of hillslope topographic asymmetry. We formulated this new model by hypothesizing that patterns in hillslope asymmetry are controlled primarily by latitude, topographic slope, mean annual temperature, and an aridity index. In this model, $HA_{\text{N-S}}$ values are predicted using

$$HA_{N-S} = \begin{cases} I_A S^b \sin\left(\dfrac{\pi\varphi}{180^\circ}\right) & \text{if } T > T_g \\ -I_A S^b \sin\left(\dfrac{\pi\varphi}{180^\circ}\right) & \text{if } T \leq T_g \end{cases} \quad (1)$$

where I_A is the aridity index (defined as the ratio of potential evapotranspiration to precipitation), S is the average slope gradient, b is an exponent between 0 and 1, φ is latitude, T is mean-annual temperature, and T_g is a threshold mean-annual temperature below which vegetation growth becomes substantially limited by temperature.

The model is based on a parsimonious set of equations that effectively reproduce the primary patterns in Figure 1, including the fact that hillslope asymmetry reverses at the equator and has a stronger dependence on latitude at lower latitudes (which suggests a sine dependence on latitude), correlates positively with average slope gradient (which suggests a power-law or otherwise simple algebraic dependence on average slope gradient), reverses sign in the mid latitudes where a critical elevation is exceeded (one that correlates with mean annual temperature falling into single digits where temperature becomes a limiting factor for vegetation growth) and correlates positively with aridity (which we have reproduced using a linear dependence on the aridity index).

The purpose of this model is to demonstrate that broad-scale spatial variations in topographic asymmetry on hillslopes can be reproduced with just a few variables that relate to differential insolation (i.e. latitude and slope gradient), water availability (i.e. the aridity index), and mean-annual temperature. Moreover, the model provides a useful unifying theme for the conceptual model that explores the feedbacks among CZ processes.

Average slope gradient, computed from the global SRTM DEM at 3 arc-second resolution, is included in the model to represent the fact that gently sloping landscapes have smaller differences in insolation between pole- and equator-facing hillslopes, hence the positive feedbacks that drive hillslope asymmetry are likely not as strong in such cases. For the map in Figure 2 we assumed $b = ½$. We used a value less than 1 in order to represent the fact that, while steeper slopes have larger differences in insolation between pole- and equator-facing hillslopes that can drive the feedbacks in CZ processes that lead to topographic asymmetry, steeper slopes also tend to have thinner soils, which can be expected to somewhat lessen the magnitude of such feedbacks. The value of b influences the relative magnitude of $HA_{\text{N-S}}$ as a function of local relief, but it does not control the spatial patterns in the sign of $HA_{\text{N-S}}$ that we emphasize here.

Global grids of mean-annual temperature, T, and the aridity index, I_A, at 30 arc-second resolution were sourced from Hijmans *et al.* (2005) and Zomer *et al.* (2008), respectively (note that Zomer *et al.* define the aridity index inversely relative to our definition). The temperature at which vegetation growth becomes substantially limited varies from species to species and on precisely how the growth limitation is defined. Figure 1 was created assuming a T_g value of 5°C. This value was chosen because a temperature growth threshold of approximately 5°C has been documented for Douglas fir (Emmingham, 1977; Bailey and Harrington, 2006) and other northern hemisphere conifer species (Schönenberger and Frey, 1988; Deslauriers *et al.*, 2003; Rossi *et al.*, 2007). As such, 5°C is likely broadly representative of the threshold temperature below which vegetation growth in conifer forests becomes substantially limited. Decreasing the value of T_g has the effect of expanding the range in which pole-facing hillslopes are steeper than equator-facing hillslopes to higher latitudes and elevations. The aridity index is included to reflect the fact that the difference in drought stress tends to be larger between pole- and equator-facing hillslopes in more arid climates compared with more humid climates. The value of the aridity index diverges in hyperarid climates because the denominator in the ratio become very small. For Figure 1 we limited the value of I_A to a maximum of 3 before input into Equation (1). The sine function of latitude was chosen as the simplest means of representing the increasing difference in insolation between pole- and equator-facing hillslopes with increasing distance from the equator.

Figures 1 and 2 focus on the asymmetry between pole- and equator-facing hillslopes. It is important to note, however, that the largest difference in vegetation cover and slope gradients is generally documented between northeast-facing and southwest-facing hillslopes in the Northern Hemisphere and between southeast-facing and northwest-facing hillslopes in the Southern Hemisphere. This additional east–west asymmetry has been well established in the ecological community for decades (Boyko, 1947; Perring, 1959; Holland and Steyn, 1975; Radcliffe and Lefevre, 1981; Desta *et al.*, 2004). That is, the driest hillslopes with the least vegetation cover tend to occur not on hillslopes that face directly equatorward but rather on hillslopes that face equatorward but also have a west-facing component. Poulos *et al.* (2012) quantified east–west asymmetry and found patterns consistent with a predominantly northeast–southwest slope aspect dichotomy in the Northern American Cordillera and a southeast–northwest dichotomy in the Southern American Cordillera. Pelletier and Swetnam (2017) proposed that the westward shift in minimum soil moisture and the tendency toward cliff formation under thin soil cover in their study sites in Northern Arizona and Southern Utah was the result of the warmer afternoon temperatures when southwest-facing hillslopes experience peak insolation together with the fact that evapotranspiration rate depends on the product of insolation and temperature.

Figure 3 presents a map showing where Equation (1) predicts correct and incorrect signs of $HA_{\text{N-S}}$. Clearly there are many places where the model fails to predict even the correct sign of asymmetry. Many of these places are associated with process zones that are not predominantly hillslope-fluvial in nature. For example, areas of the northeastern USA covered by the Laurentide Ice Sheet at the Last Glacial Maximum contain many locations where the model predicts the wrong sign, likely due to the impact of glacial erosion. Similarly, some areas of alpine glacial erosion, including the highest elevations of the Olympic and Big Horn Mountains for example, have a sign of asymmetry that differs from the model prediction. The Sand

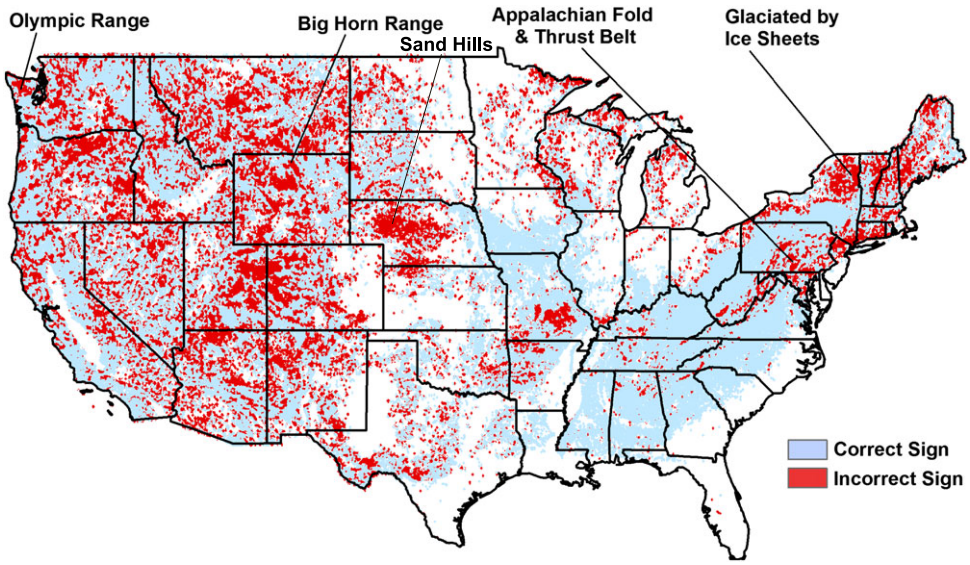

Figure 3. Map illustrating where Equation (1) predicts correct and incorrect signs of $HA_{N\text{-}S}$. Location names are provided to complement discussion in the text. [Colour figure can be viewed at wileyonlinelibrary.com]

Hills of Nebraska are primarily aeolian in nature, with topographic asymmetry that is most likely related to paleowind directions rather than to microclimate. Bedrock attributes such as lithology, the strikes and dips of strata in sedimentary rocks and bands in metamorphic rocks, and joint orientations can also contribute to asymmetry. Spatial variations in these properties likely drive some of the small-scale variability in asymmetry that is common in the western USA. Bedrock attributes may also be an important factor in controlling $HA_{N\text{-}S}$ values in the Appalachian fold and thrust belt. A full accounting of the effects of bedrock attributes on asymmetry is needed and will likely require the integration of regional and global datasets for lithology and bedrock structural attributes with DEM analyses of the kind used to produce Figure 1. The Discussion section contains additional information on the non-climatic causes of asymmetry and cases that are otherwise not well represented by the model.

Conceptual model

Summary of the model

The results presented above suggest that water-limited and temperature-limited cases can be useful end members for understanding the development of topographic asymmetry and how it varies spatially at regional to global scales. In order to understand how topographic asymmetry develops via feedbacks among CZ processes, in this section we focus down to the scale of individual hillslopes, interacting with low-order fluvial channels, as they evolve over short- and long-timescales.

Figure 4(a) and 4(b) illustrate our conceptual model for the slope aspect control of CZ development in water-limited and temperature-limited end-member cases, respectively. In each of the following subsections we draw from the literature to explore and defend the conceptual model presented in Figure 4.

The water-limited case is characterized by lower mean-annual potential evapotranspiration (PET) and actual evapotranspiration (AET) rates on northeast-facing hillslopes in the Northern Hemisphere and southeast-facing hillslopes in the Southern Hemisphere. In order to simplify the language, we will hereafter use the terminology of pole- and equator-facing hillslopes, bearing in mind that there is a significant westward component to the aspects with the highest mean PET rates. The lower mean PET rates on pole-facing hillslopes results in more available soil water, more vegetation cover, and faster soil production (Pelletier and Rasmussen, 2009) in water-limited cases, since all of these processes are positively correlated with water availability (Figure 4).

Greater vegetation cover on pole-facing hillslopes also increases dust interception (Giorgi, 1988) and hence greater potential accumulation of fine grained (clay- and silt-sized) aeolian material, and, in warm, water-limited environments, accumulation of aeolian $CaCO_3$ in the soil. This, in turn, tends to increase the water-holding capacity of pole-facing hillslopes (Gutiérrez-Jurado *et al.*, 2013). Higher rates of bioturbation and lower rates of erosion by overland flow tend to decrease the drainage density on pole-facing hillslopes, all else being equal. The slope gradient decreases on the equator-facing side due to both higher drainage density and divide migration (Istanbulluoglu *et al.*, 2008; Yetemen *et al.*, 2010). In other words, the gradient asymmetry reflects greater efficiency of downslope transport on equator-facing slopes, such that equal rates of downslope transport and hillslope erosion occur when the pole-facing hillslopes are steeper than adjacent equator-facing hillslopes.

Inputs to the Critical Zone

The mean-annual insolation entering the CZ at the top of the plant canopy tends to be higher on equator-facing hillslopes relative to pole-facing hillslopes (illustrated using darker colors/more shading on pole-facing hillslopes in Figure 4). This difference in incoming energy as a function of slope aspect and gradient is the fundamental driver of topographic asymmetry in both the water- and temperature-limited cases illustrated in Figure 4. In water-limited cases, higher mean-annual insolation on equator-facing hillslopes increases surface temperatures (illustrated using a thermometer) and ET rates (illustrated using squiggly blue curves of varying thickness and length), leading to lower mean soil moisture (illustrated as less blue in the soil) as described in the subsection below on water balance. Lower soil moisture, in turn, triggers a cascade of feedbacks among CZ processes, detailed in the following subsections, which lead to asymmetry in many CZ states and fluxes between pole- and equator-facing hillslopes. If temperatures are sufficiently low, vegetation growth can become limited. In such cases,

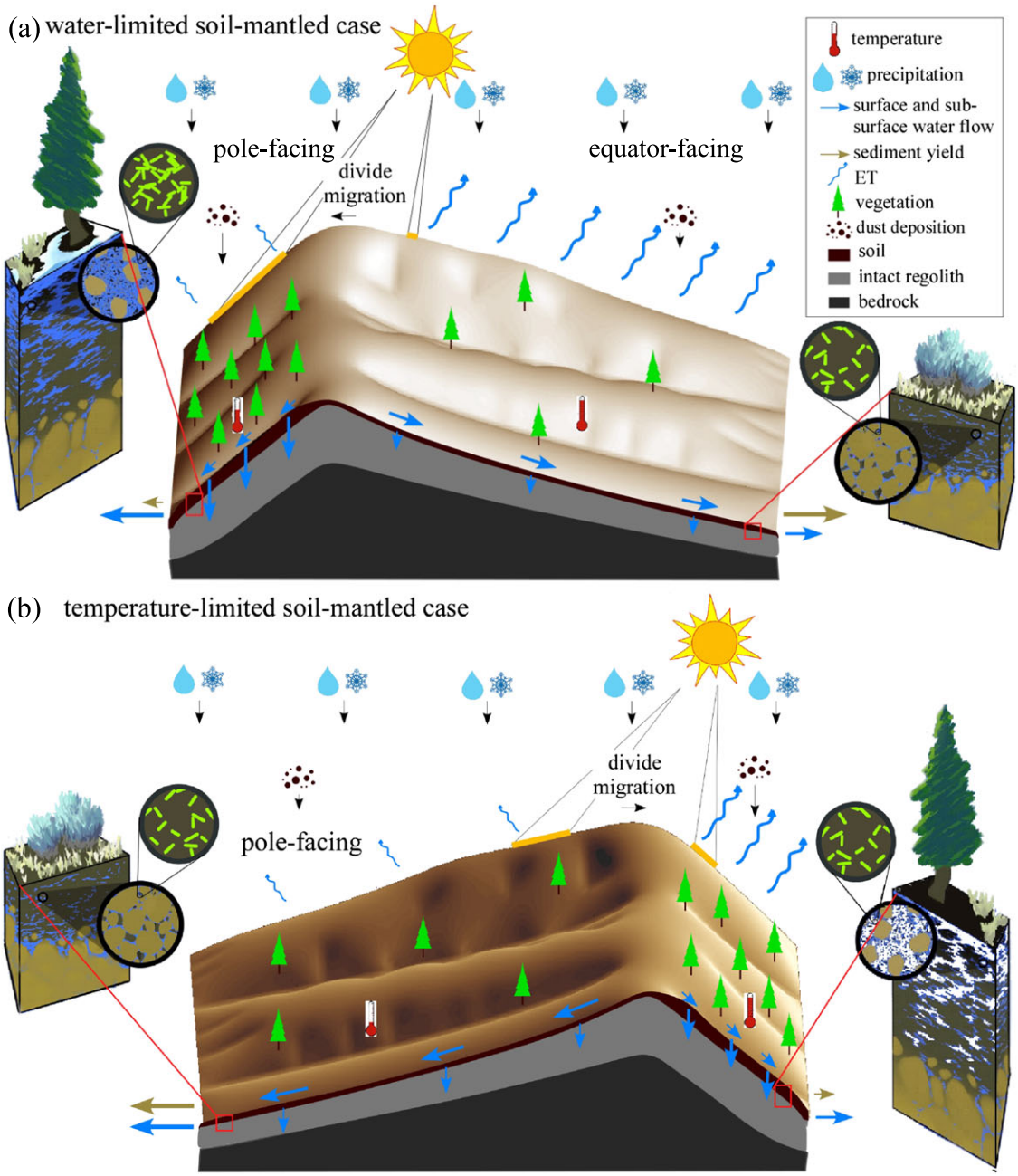

Figure 4. Conceptual models for (A) water-limited and (B) temperature-limited soil-mantled cases. Blue represents water in soil pore spaces while white represents air. In (A), soils are poorly developed on equator-facing hillslopes, limiting water storage potential. In (B), soils are more well developed on equator-facing hillslopes but higher PET results in lower water storage. [Colour figure can be viewed at wileyonlinelibrary.com]

vegetation will grow more rapidly on the relatively warm equator-facing hillslopes despite the lower soil moisture on those slopes. Greater vegetation cover and warmer temperatures can lead to the development of thicker soils on equator-facing hillslopes despite generally drier conditions.

The seasonality and diurnal variation of insolation can be critical to understanding CZ dynamics. For example, the insolation during wet seasons – whether snow- or rain-dominated – likely exerts more control on the CZ water balance than insolation during dry seasons. Yetemen *et al.* (2015b) documented the annual variation in insolation on pole- and equator-facing hillslopes at a range of latitudes. Resolving such variations can be important when considering water inputs that are highly seasonal. Diurnal timing of insolation is important as well, with insolation exacerbating moisture stress more in the warm afternoons on more westerly aspects, and less in the morning on easterly aspects (Pelletier and Swetnam, 2017).

Several empirical models predict PET as a function of insolation. Evapotranspiration equations that combine energy balance and turbulent transfer such as the Penman–Monteith and Priestley–Taylor equations use radiation and air temperature. One of the simplest methods is that of Hargreaves and Samani (1985), who related PET rates to the product of insolation and a nonlinear function of air temperature. The fact that PET depends on the product of insolation and a nonlinear function of air temperature implies that the diurnal cycle should generally be taken into account in slope aspect studies (e.g. warmer temperatures in the afternoon result in higher PET on west-facing hillslopes compared with east-facing hillslopes).

Given that inputs to the CZ include two very different types, i.e., mass and energy, methods have been developed to place these types into a common energy-based currency. For example, the Effective Energy and Mass Transfer (EEMT) approach of Rasmussen *et al.* (2015) quantifies the water input to the CZ via the heat energy content of that water, multiplying the

water flux by a temperature and a unit specific heat. Similarly, net primary production (NPP) is quantified in terms of energy using an enthalpy term. The EEMT approach has an explicit slope aspect dependence via the effect of insolation on PET rates. EEMT has been used as a theoretical framework for understanding the slope aspect dependencies of many CZ states and fluxes, including soil production rates, differences in above-ground biomass, hillslope-scale relief, drainage density, soil thickness, and water transit times (Pelletier and Rasmussen, 2009; Pelletier *et al.*, 2013; Zapata-Rios et al., 2015a, 2015b).

CZ development involves timescales longer than the Holocene. As such, in some cases the climate of the latest Pleistocene may be as relevant or more relevant than the modern climate in controlling the current state of the CZ (McGuire *et al.*, 2014). Late Pleistocene climates were colder than Holocene climates, with the temperature difference between the Holocene and Last Glacial Maximum greater at higher latitudes and closer to the Laurentide and Fennoscandian ice sheets compared with lower latitudes (Thompson *et al.*, 1993). Climates were generally drier at LGM compared with the Holocene, but some regions (e.g. the southwestern USA) are important exceptions to this general trend (Thompson *et al.*, 1993). Temperature and precipitation both control vegetation cover, which influences many CZ processes as described in the following subsections. The LGM was also a dustier world than today (Mahowald *et al.*, 1999), with potentially important implications for rates of pedogenesis.

Some slope aspect studies have explicitly invoked paleoclimatic conditions as essential for understanding the modern state of the CZ. For example, Anderson *et al.* (2013) developed a hillslope evolution model that combined rock damage due to frost cracking, and downslope transport of mobile regolith by repeated frost heave and thawing. Their model predicted that bedrock would be more heavily and deeply damaged on pole-facing hillslopes, due to the reduced rock temperature, especially during the colder climates that dominate the late Quaternary. McGuire *et al.* (2014) found that pole-facing hillslopes on cinder cones of a given age were steeper, and therefore experienced lower rates of erosion, relative to adjacent south-facing hillslopes. McGuire *et al.* (2014) noted that, due to the asymmetric nature of glacial/interglacial transitions, the climate state most relevant for interpreting the evolution of cinder cones older than approximately 50 ka is the glacial climate. Using paleovegetation modeling, McGuire *et al.* (2014) demonstrated that vegetation cover was likely reversed for the cinder cones in Arizona, i.e. for most of the Quaternary, pole-facing hillslopes were temperature-limited and near the upper tree line, whereas equator-facing hillslopes likely had greater vegetation cover. Therefore, the reduced steepness of equator-facing hillslope can be attributed to increased rates of bioturbation relative to pole-facing hillslopes during the predominantly glacial climates of the Pleistocene.

Water balance

Recent efforts at sites within the Critical Zone Observatory (CZO) network have highlighted the differences among mechanisms affecting water partitioning on pole- and equator-facing hillslopes. Generally, pole-facing hillslopes have denser vegetation cover and receive less incoming solar radiation, resulting in higher evapotranspiration rates than pole-facing hillslopes (Figure 4). Thicker soils and regolith on pole-facing hillslopes generally lead to higher infiltration rates, longer water residence times, and more baseflow to streams than on equator-facing hillslopes, as observed at the Jemez-Catalina CZO (Broxton *et al.*, 2009; Zapata-Rios et al., 2015a, 2015b). In Figure 4, blue lines with arrows illustrate rainfall-runoff partitioning. On equator-facing hillslopes, more of the incoming precipitation is lost to ET. As such, less water is available for runoff and infiltration on these hillslopes. The interactions among vegetation cover, regolith/soil development, and subsurface water flow that lead to sparser vegetation, thinner regolith/soil, and less subsurface available water represents a key positive feedback in the CZ.

Importantly, the relative impact of slope aspect on water inputs is dynamic across an annual cycle based on apparent solar angle differences in winter versus summer months. As such, aspect-derived differences in insolation inputs are greatest during the winter when snow is the primary form of precipitation in many montane ecosystems, and differences are lowest during summer seasons characterized by either rainy or dry conditions (Zou *et al.*, 2007). The consequences of these patterns can be significant in areas that receive even modest winter snow. For example, in both the Boulder Creek Critical Zone Observatory (BcCZO) and the Catalina-Jemez Critical Zone Observatory (SCM-JRB CZO), pole-facing hillslopes develop a seasonal snowpack throughout the winter that melts in spring, while the equator-facing hillslopes do not accumulate a snowpack. Instead, pulsed accumulation and melt occurs over short timescales (hours to days) across the period of snowfall. In water-limited cases (Figure 4(a)), this causes slope aspect to alter the timing of snowmelt (Tague and Peng, 2013; Harpold *et al.*, 2014; Harpold, 2016). Langston *et al.* (2015) found that the contrast in snowmelt timing corresponded to a contrast in late winter to early spring soil moisture in the BcCZO. Their calculations with a vadose-zone flow model suggested the potential for prolonged snowmelt on pole-facing slopes to drive a higher meltwater flux below the root zone. Hinckley *et al.* (2014b) found that pole-facing hillslopes exhibit lateral subsurface flow through a connected matrix during snowmelt, which may be driven by periodic refreezing in the subsurface or fracture orientation parallel to the slope (Bandler, 2016). In contrast, equator-facing hillslopes have two domains of flow: rapid vertical transport during snowmelt and little water movement through a disconnected soil matrix between events. Here, periods of rapid vertical flow may be driven by the rate and amount of water supply, as well as the orientation of subsurface fractures perpendicular to the slope (Bandler, 2016).

During summer months in mid-elevation mountainous catchments, the distinction between aspects is less apparent in terms of differences in sun angle. For example, at the BcCZO, Hinckley *et al.* (2017) observed sub-meter scale heterogeneity in soil moisture and the fate of nitrogen (N) across both pole- and equator-facing hillslopes throughout the summer months, leading to no significant difference between aspects. Only during rainfall events did they observe higher infiltration rates due to a more connected soil matrix on pole- than equator-facing hillslopes. In general, across seasons, pole-facing hillslopes provide quicker and more efficient movement of water through the subsurface than equator-facing hillslopes, in part due to differences in evolved soil properties (e.g., organic matter content).

Vegetation

The distribution of vegetation on landscapes (ecosystem structure) is driven in part by abiotic factors, i.e. slope aspect and soil type, which are expressed as stressors or facilitators (ecosystem function) of individual health, size, and reproductive rate. Conversely, ecosystem structure reduces the surface energy budget by shielding and shading the surface of the soil (Zou *et al.*, 2007; Bode et al., 2014). On pole-facing hillslopes

in water-limited cases (Figure 4(a)), ecosystem structure generally exhibits larger accumulations in standing biomass and deeper accumulations of organic detritus. These accumulations are due in part to reduced ET rates and greater soil water availability than on equator-facing hillslopes, resulting in greater NPP. In temperature-limited cases (Figure 4(b)), equator-facing hillslopes have relatively more standing biomass than pole-facing aspects due to the reduction in degree growing days, which limit metabolic function.

Ecosystem structure can affect the water budget through leaf-level transpiration, reduced soil evaporation due to shading altering snow and patterns of sublimation (Gustafson *et al.*, 2010) and rates of snowmelt (Molotch *et al.*, 2009; Harpold *et al.*, 2014), the vertical redistribution of water in the subsurface (Quijano and Kumar, 2015), and overall available moisture by way of ET partitioning (Breshears *et al.*, 1998). Vegetation sequesters atmospheric carbon and nitrogen, emitting numerous complex organic and inorganic molecules back into the CZ, further altering CZ processes. These organic and inorganic feedbacks, changes in energy budget and water cycling, and bioturbation are important drivers of CZ evolution at both short- and long- timescales. All of the short-timescale inputs described above serve as drivers within the EEMT model (see subsection on inputs to the Critical Zone) and are a means by which one can numerically acknowledge the role of vegetative cover in influencing CZ evolution.

At moderate timescales, slope aspect influences rates of ecosystem carbon (C) uptake by altering plant root available soil water, air and soil temperature, and total incident solar radiation, as summarized by Eamus (2003). In an eastern North American deciduous forest, Desta *et al.* (2004) found biomass was 25-50% greater, mean annual temperature was 5.5°C cooler, and vapor pressure was 37% lower on pole- than equator-facing aspects. The aridity index, described in the first section as the ratio of PET to precipitation, is a relative rather than absolute value and neglects the actual evapotranspiration (AET) experienced by plants. Stephenson (1990) found AET and vapor pressure deficit (VPD) are the most biologically meaningful correlates to biomass in a water-limited Sierra Nevada forest – representing a means by which the lithosphere (by way of aspect) can drive heterogeneity in ecosystem function. In temperature-limited cases (Figure 4(b)), slope aspect alters the number of degree growing days for photosynthesis and the rates at which optimal C assimilation can take place. This is true at both the leaf-scale in terms of C assimilation through photosynthesis, transpirational water loss, and the resulting water use efficiency and at the ecosystem scale in terms of annual NPP (Chen *et al.*, 2007).

Vegetation and biomass also have indirect effects on CZ function over long (i.e., millennial) timescales, which ultimately influence the mean-annual water balance, accumulation of belowground biomass, and the accretion of biological C into soils. Spatial variability in the patterns of biomass by slope aspect have long been reported by ecologists working in complex terrain; most notably the seminal work by Whittaker and Niering, 1965, 1975; Whittaker *et al.*, 1968; Day and Monk (1974), and Armesto and Martínez (1978). The establishment of mature steady-state forests takes hundreds of years to millennia, in synchrony with natural climatic variation (Swetnam and Betancourt, 1998).

The influence of vegetation and slope aspect on natural hazards includes (but is not exhaustively limited to): wildfire spread and severity (Taylor and Skinner, 1998; Heyerdahl *et al.*, 2001; Bradstock *et al.*, 2010; Wood *et al.*, 2011), debris flows (Gabet and Dunne, 2002; Rengers *et al.*, 2016), and invasive species establishment (Bradley and Mustard, 2006; Van Devender and Dimmitt, 2006).

Biogeochemical processes

For most studies that have evaluated biogeochemical stocks and processes on pole- versus equator-facing hillslopes, aspect is treated as a template that provides contrasting conditions, which, in turn, drive variations in ET rates (Hargreaves and Samani, 1985) and therefore soil C and nutrient cycling rates (Kang et al., 2003; Stielstra *et al.*, 2015). For example, pole-facing hillslopes generally favor conditions that promote higher storage of soil C and nitrogen (N) (Kunkel *et al.*, 2011): deeper regolith, higher microbial biomass and accumulation of organic matter (microbial biomass is illustrated using green-colored microbes in the microscale insets of Figure 4). Hinckley *et al.* (2014a) found higher uptake of N inputs by microbes during spring snowmelt on pole- than equator-facing hillslopes. They attributed this difference to slower, sustained melting of a seasonal snowpack (releasing N-rich meltwaters to the subsurface) on pole-facing hillslopes, and rapid vertical flow of meltwater and N on equator-facing hillslopes. During summer months, when soil moisture was heterogeneous across both aspects, Hinckley *et al.* (2017) found evidence of equally heterogeneous N transformations (especially nitrification) that was not aspect-dependent.

Despite patchiness across both aspects during dry periods, there is strong evidence that a more connected soil matrix that rapidly distributes water, C, and nutrients in the subsurface during precipitation events characterizes pole-facing hillslopes. This connectivity is 'sustained' during the period of snowmelt (in snow-dominant) regions and into the start of drier summer months. By contrast, equator-facing hillslopes seem to have more of a 'boom and bust' cycle, with heterogeneous, rapid vertical flow occurring at sub-meter scales, and patchy vegetation. Hot spots and hot moments (McClain *et al.*, 2003) are often a topic of interest in biogeochemical studies, as they describe times or locations of disproportionate importance within ecosystems. These places and times may occur more often on equator- than pole-facing hillslopes, as there is a build-up of material when soils dry down completely between events (snowmelt or rainfall) or in space, such as in a patch of grasses versus bare ground. When water is added, a pulse of microbial activity may occur, such as soil CO_2 flux (Barron-Gafford *et al.*, 2011), constituting a hot moment that can be incorporated into a numerical representation of soil C dynamics, available moisture, and microbial activity (Zhang *et al.*, 2014). Similarly, patchiness in microbial communities and plant material across space on equator-facing hillslopes likely results in hot spots, but in general, this remains understudied. For example, Belnap *et al.* (2005) describe this type of behavior for desert landscapes characterized by sub-meter scale heterogeneity in ecological communities, but they only discuss that aspect plays a role rather than study it explicitly.

Pedogenesis

Properties of the soil that are relevant for storing water and supporting life include the thickness of soil above bedrock or intact regolith and the textural, mineralogical, and organic properties of that soil. Vegetation cover controls the rate of dust deposition for a given atmospheric dust concentration, since dust that migrates below a taller, denser plant canopy is more likely to be deposited and retained compared with dust migrating below a short and/or open canopy (Giorgi, 1988). As such, soil development is thought to operate in positive feedback with vegetation in water-limited environments such that pole-facing hillslopes have thicker soils and a higher concentration of fine particles in the soil matrix that lead to greater water-

holding capacity and more above-ground biomass in a positive feedback (Figure 4(a)). Thicker soils with higher silt-clay and organic matter contents have been documented on pole-facing hillslopes in the water-limited cases of Dry Creek Experimental Watershed (Geroy *et al.*, 2011; Smith *et al.*, 2011), the BcCZO (Foster *et al.*, 2015), the SCM-JRB CZO (Lybrand *et al.*, 2011; Pelletier *et al.*, 2013; Olyphant *et al.*, 2016) and many more humid study sites (Losche et al., 1970; Daniels et al., 1987a, 1987b; Carter and Ciolkosz, 1991; Bale *et al.*, 1998; Begum *et al.*, 2010). However, these studies also indicate equator-facing hillslopes exhibit a greater degree of chemical weathering in terms of the mineral composition of the secondary clays, evidence of clay translocation and argillic horizon formation, and greater pedogenic Fe-oxide accumulation and loss of mobile cations often not present on pole-facing hillslopes. The slope aspect differences appear to be largely a function of temperature, with increased soil moisture and primary production leading to greater organic matter input and accumulation on pole-facing hillslopes, but an enhanced chemical weathering on equator facing hillslopes as a result of warmer temperatures. Warm, water-limited locations also exhibit greater organic matter accumulation on pole-facing hillslopes, but appear not to exhibit greater chemical weathering on equator-facing hillslopes, and indeed may exhibit accumulation of soluble salts under semiarid to arid conditions (Kutiel, 1992; Kutiel and Lavee, 1999). Interestingly, the control of slope aspect on soil properties appears to diminish and not play a major role grading towards arid and hyper-arid climates (Kutiel and Lavee, 1999). This may be another indicator of the importance of variable vegetation cover in driving slope-aspect variations, as arid and hyper-arid climates may have equally sparse vegetation cover on both pole- and equator-facing hillslopes.

Soil properties also exhibit clear slope aspect relationships in mid- to high-latitude locations that have mean-annual temperatures less than approximately 5°C, but that differ in part from those of their warmer counterparts (Macyk et al., 1978; Hunckler and Schaetzl, 1997; Egli *et al.*, 2006, 2015; Eger and Hewitt, 2008). Specifically, pole-facing hillslopes exhibit thicker soils, increased organic matter accumulation, and greater leaching intensity, chemical weathering and podsolization relative to equator-facing hillslopes. The slope aspect variation in soil properties in these systems appears to be controlled by the relative duration of snowpack and its impact on soil moisture, primary production and freeze–thaw activity. Equator-facing hillslopes exhibit more frequent variation in amount and depth of snowpack, with greater loss to melting and sublimation. The loss of snowpack reduces the amount of water available to flush through the soil profile and allows for greater freeze–thaw activity on the equator-facing hillslopes. The relative lack of moisture limits primary production and the downward flush of dissolved organic carbon and weathering products. Interestingly, Egli *et al.* (2015) demonstrated that in very cold locations with permafrost in the Altai Mountains near the Russia–Mongolia–China border, pole-facing hillslopes still exhibited a greater degree of chemical weathering. These authors hypothesized that temperature was not the limiting factor in terms of chemical weathering, in that all locations were very cold with mean-annual temperatures <0°C, but that the greater snow pack on pole-facing hillslopes limited organic matter decomposition allowing for accumulation of highly mobile low molecular weight organic ligands that facilitate chemical weathering and downward translocation of Fe and Al.

Soil development is controlled, in part, by the thickness of intact regolith, since regolith formation prepares the parent material for faster soil development once it is entrained into the mobile layer. Regolith thickness is deeper on pole-facing hillslopes in the BcCZO (Befus *et al.*, 2011) and the SCM-JRB CZO (Olyphant *et al.*, 2016). This is consistent with the hypothesis that regolith thickness is, in part, controlled by water availability (Lebedeva and Brantley, 2013) and vegetation cover. Recent research has demonstrated the importance of other factors, such as topographically induced stresses (Holbrook *et al.*, 2014; St. Clair *et al.*, 2015) and water table depth (Rempe and Dietrich, 2014) on regolith thickness.

Topographic development

The sediment transport processes on soil-mantled hillslopes can be grouped into (1) local disturbance processes that lead to a net downslope movement of sediment in small increments (e.g. freeze–thaw-driven creep, bioturbation, rainsplash) which collectively tend to smooth landscapes, and (2) erosion by surface runoff, which tends to incise landscapes via the positive feedback between contributing area and incision rate. The transition from soil-mantled hillslopes to low-order fluvial valleys is defined by a shift in process dominance from processes that smooth to those that incise (Tarboton, 1992; Perron *et al.*, 2008). As such, we can conclude that diffusive processes are dominant on hillslopes. However, topographic asymmetry likely arises in many cases (e.g. Figure 4) from a combination of diffusive processes and surface runoff that interact to create disparities in erosion rates and drive drainage divide migration. Nonetheless, it is useful to examine the effect of slope aspect on the efficiency of diffusive processes. Efficiency in this context is closely related to the value of the topographic diffusivity or, equivalently, the rate of sediment transport on hillslopes for a given slope.

Imbalances in erosion rates due to a greater efficiency of diffusive processes on equator-facing hillslopes will cause a relative steepening of pole-facing hillslopes (Figure 4). Although some studies have begun to address how rates of rainsplash vary with particle size, raindrop properties, and vegetation cover (Gabet and Dunne, 2003; Dunne *et al.*, 2010) and how soil thickness and rates of bioturbation vary with vegetation type (Gabet *et al.*, 2003; Yoo *et al.*, 2005; Hughes *et al.*, 2009; Winchell *et al.*, 2016), we currently lack the ability to quantify the relative importance of these processes over geologic timescales most relevant to the development of hillslope topography. However, rainsplash and discontinuous overland flow are likely only a significant portion of the total sediment transport on landscapes with substantial bare ground, such as in a shrub-dominated landscapes or after a disturbance such as a wildfire. Therefore, creep and bioturbation are likely the most important transport mechanisms on most soil-mantled hillslopes.

In addition to increasing or decreasing the efficiency of creep and bioturbation, slope aspect can drive spatial variations in diffusive sediment transport by influencing the thickness of soil or mobile regolith. Diffusive soil transport processes have been argued to be a function of soil thickness up to some limiting value (Heimsath *et al.*, 2005; Roering, 2008; Pelletier *et al.*, 2011; Johnstone and Hilley, 2015). On water-limited hillslopes, the thickness of soil is generally greater on pole-facing hillslopes relative to equator-facing hillslopes. This can increase sediment transport in a positive feedback, i.e. an increase in the thickness of the mobile soil column will cause an increase in soil flux unless the mean velocity decreases proportionally.

Where the contribution of diffusive processes to the overall erosion rate dominates that from surface runoff, topographic asymmetry may be attributed solely to variations in the

efficiency of diffusive processes. However, the more general conceptual model developed here considers the interaction of hillslopes with low-order fluvial valleys (Figure 4). In these settings, diffusive processes play an important role in determining drainage density as well as channel head and drainage divide migration. In particular, greater efficiency of bioturbation combined with lower efficiency of erosion by overland flow on forested slopes can promote differences in drainage density on opposing slopes, leading to divide migration and topographic asymmetry. However, drainage density tends to increase with slope in addition to the efficiency of colluvial transport processes (Perron *et al.*, 2008), hence the steeper slopes characteristic of pole-facing slopes in the water-limited case (and of equator-facing slopes in the temperature-limited case) can offset this greater efficiency and cause drainage density to be approximately equal on nearby hillslopes of opposing aspect.

The role of vegetation on the partitioning of flow shear stress between bed sediments and vegetation biomass has been studied in laboratory experiments and natural rivers (Nepf, 2012; Le Bouteiller and Venditti, 2015). These observations have been used to adapt earlier theory for grain and form resistance by introducing vegetation properties, such as biomass and stem height and diameter, as input to shear stress partitioning formulations. Yetemen et al. (2015a, 2015b) used one such formulation, which inversely relates shear stress to biomass, in the CHILD landscape evolution model. In CHILD, an ecohydrology model of vegetation dynamics and runoff generation driven by spatial solar radiation and stochastic arrivals of storm pulses is coupled with a shear-stress-dependent fluvial erosion model and a nonlinear creep equation. On an evolving topography driven by semiarid climatology of the southwestern USA, relating shear stress to biomass led to emergent patterns in topographic structure, vegetation biomass, as well as the spatio-temporal behavior of soil moisture and vegetation dynamics, mediated by the rate of uplift (Yetemen *et al.*, 2015a). Hillslope asymmetry emerged in the model with steeper pole-facing slopes with higher plant biomass and less steep equator-facing slopes with lower plant biomass. Modeled hillslope asymmetry was consistent with calculated values from a 10 m pixel^{-1} Digital Elevation Model (DEM). An interesting outcome of the model was the emergence of hysteresis of soil moisture and spatial variability in vegetation patterns, in which the spatial variability of soil moisture and vegetation biomass during wetting and drying phases follows different trajectories switching from network flow-path control during wettest times of the year to aspect control, generally consistent with ecohydrologic studies (Mascaro and Vivoni, 2016).

Extreme events

In some cases, slope aspect driven changes to vegetation, soil, or bedrock properties can lead to spatial variations in the factors that drive and resist sediment transport, making one slope aspect more likely than another to cross a critical geomorphic threshold in response to an extreme event. For example, an extreme rainfall event in 2013 triggered more than 1138 debris flows in the Colorado Front Range, with 78% occurring on water-limited, sparsely vegetated south-facing hillslopes (Coe *et al.*, 2014). Anderson *et al.* (2015) estimated that debris flows triggered during this 2013 rainstorm resulted in the removal of hundreds to thousands of years of weathered regolith at their study area in the Colorado Front Range west of Boulder, CO. A pair of recent studies concluded that spatial variations in apparent root cohesion conferred by vegetation were most likely responsible for the aspect control on debris flow initiation (McGuire *et al.*, 2016; Rengers *et al.*, 2016). In addition, Ebel *et al.* (2015) documented that soils became saturated on south-facing hillslopes during the same 2013 rainstorm while remaining unsaturated on north-facing hillslopes at their study site near the 2010 Fourmile Canyon fire. They attributed the aspect-driven variation in hydrologic response to lower weathered-bedrock permeability and a higher gravel/stone fraction on south-facing hillslopes relative to north-facing hillslopes, illustrating how long-term feedbacks between CZ processes and slope aspect may also contribute to debris flow susceptibility.

More generally, our understanding of links between short- and long-timescale processes within the context of sediment transport is limited by uncertainty regarding the relative contribution to overall erosion rates that stem from continuously operating transport processes (e.g. creep) and infrequent events (e.g. severe drought, extreme rainfall, wildfire) that can trigger pulses of rapid sediment transport. There is growing evidence that sediment transport occurring within a short time period following a disturbance event, such as wildfire, may account for the majority of landscape denudation over geologic timescales in certain settings. Pelletier and Orem (2014) documented how wildfire severity influenced post-fire erosion by slope and contributing area, concluding in Orem and Pelletier (2016), that up to 90% of the erosion from a water-limited soil mantled landscape was caused by historical wildfires. Therefore, it is necessary to consider how slope-aspect-driven variations in CZ processes may modulate a landscape's response to such disturbances. Wildfires, for example, lead to a substantial increase in runoff-generated debris flows relative to similar unburned areas or those burned at low severity. In the years following wildfire, an increased risk of shallow landslides on steep slopes could result from a loss of apparent cohesion associated with a decay in root network strength (Schmidt *et al.*, 2001; Jackson and Roering, 2009) or an increased likelihood of soil saturation associated with decreases in canopy interception. Additionally, reductions in soil infiltration capacity, which can be linked to wildfire severity (Moody *et al.*, 2016), lead to large increases in runoff-driven erosion relative to unburned areas (Inbar *et al.*, 1997; Shakesby and Doerr, 2006). Since surface energy budget changes by slope aspect can increase the fireline intensity during a wildfire event (Bradstock et al., 2010; Wood *et al.*, 2011), aspect has the potential to influence the spatial distribution of landslides and runoff-driven soil erosion within recovering burned areas. Further work addressing the settings in which rare events, such as wildfire followed by intense rainfall, are likely to accentuate or combat the aspect-driven feedbacks existing under typical conditions (Figure 4) would aid in linking short- and long-term processes.

Exploration of the conceptual model with Landlab and the Terrestrial Integrated Modeling System (TIMS)

Appendices A and B present the results of numerical models that capture some of the long-timescale and short-timescale elements, respectively, of the conceptual model of Figure 4(a). Please note that the Landlab and TIMS models described here do not have the capability to model every process included in the conceptual model. As such, these model results are intended to demonstrate how current models capture some of the important feedbacks in CZ processes.

Appendix A describes a mathematical model that explores the feedbacks among water availability, vegetation cover, soil

development, and topographic development driven by slope-aspect differences in mean-annual insolation using a simple, aspect-dependent landform evolution model constructed using the Landlab modeling toolkit (Hobley *et al.*, 2017) (Figure 5). The question addressed in Appendix A is: Does hillslope asymmetry emerge as a landscape property by coupling steady-state models of annual biomass production driven by rainfall and solar radiation, and geomorphic transport laws that relate mean-annual rates of soil creep and fluvial incision to biomass? Figure 5 shows three modeled landscapes that embody several of the feedbacks illustrated in the conceptual model (Figure 4). These feedbacks include the linkage between aspect, insolation, ET, soil moisture, vegetation biomass, and erosional efficiency (see Appendix A for complete details). Although these are only a subset of the factors illustrated in the conceptual model of Figure 4, the ability of this simple model to reproduce the observed sense of asymmetry in water-limited regions indicates that this conceptual model is consistent with our current process-level understanding. The example also illustrates the use of such process-based models in testing the feasibility of different hypothesized mechanisms (in this case, for example, the inhibition of surface-water erosion by vegetation, and two alternative vegetation impacts on soil creep by impeding rainsplash and enhancing bioturbation). Such testing would require quantitative comparison of observed and modeled terrain characteristics, such as the slope–area curves associated with the pole- and equator-facing aspects (Figure 5, bottom row). Appendix A presents additional information on this case study. Regardless of the role of biomass in hillslope diffusion, model results show $HA_{N\text{-}S} > 0.11$ (Figure 5), consistent with the values reported by Poulos *et al.* (2012) for North America (Figure 1).

Appendix B presents a numerical experiment using the Terrestrial Integrated Modeling System (TIMS; Niu *et al.*, 2014) that compares the short-term CZ behavior for a hypothetical landscape in which the land surface is assumed to be flat for the purposes of computing insolation (FLAT) versus one that uses the radiation correction scheme (RADCOR). The question addressed in Appendix B is: Which short-term CZ processes are most affected by spatial variations in insolation related to slope aspect? TIMS integrates a surface and subsurface coupled flow model (Camporese *et al.*, 2010), a land-atmosphere energy, water, and carbon exchange scheme (Noah-MP; Niu *et al.*, 2011), and a six-carbon pool microbial enzyme model (Zhang *et al.*, 2014). The rate of gross photosynthesis is computed as the minimum of three limiting factors: Rubisco limitation, light limitation, and that associated with transport of photosynthetic products for C3 plants and PEP-carboxylase limitation for C4 plants following Farquhar *et al.* (1980) and Collatz *et al.* (1991, 1992). The six C pool model represents the controls of soil temperature and moisture on degradation of soil organic C into dissolved organic carbon (DOC) through enzymatic catalysis and assimilation of DOC into microbial biomass for growth, releasing CO_2 during respiration.

This numerical experiment was carried out using Marshall Gulch, a subhumid study site within the SCM-JRB CZO site northwest of Tucson, Arizona (32.43°N, 110.77°W). Marshall Gulch is located at high elevation (approximately 2500 m a.s.l.) so it is relatively humid compared with lower-elevation sites in Arizona and southwestern USA. However, with a mean-annual temperature of 10°C, the site is not temperature-limited.

The modeling results averaged over the entire 8 modeling years indicate that shading effects are dominant over scattering effects (Figure 6). Over the whole catchment, RADCOR produces less net (absorbed) solar radiation than does FLAT by 25% due to shading effects, with pole-facing hillslopes absorbing up to 100 W m^{-2} less solar radiation (Figure 6(a)). However, the scattering effects due to additional diffuse radiation reflected by neighboring pixels are negligible as the equator-facing hillslopes do not show much additional net solar radiation. The shading effects are then propagated to other variables, resulting in less ET (Figure 6(b)), and cooler (Figure 6(c)) and wetter surface soil (Figure 6(d)) compared with pole-facing hillslopes. Gross primary production (GPP) (Figure 6e), Leaf Area Index (LAI) (Figure 6(f)), and net ecosystem productivity (NEP) (Figure 6(g)) are reduced due mainly to the decrease in light availability despite increased soil water availability (Figure 6(d)) over the pole-facing slopes in this subhumid catchment. The microbial biomass (Figure 6(h)) and respiration fluxes (Figure 6(i)) are reduced on pole-facing hillslopes due mainly to reduced microbial activities caused by lower soil temperatures (Figure 6(c)). Appendix B presents additional details on this numerical experiment.

Discussion

Implications for our broader understanding of the Critical Zone

The conceptual model of this paper suggests that soil moisture and vegetation cover are essential to understanding CZ development across timescales. Moisture availability is crucial as water acts as a catalyst in nearly all CZ processes, and vegetation, which depends on water availability in all but the most humid and/or temperature stressed environments, plays important roles in producing regolith from bedrock and controlling the water balance. Brantley *et al.* (2017), for example, have emphasized the importance of vegetation as 'builders and plumbers' of the CZ. The importance of soil moisture and vegetation underscore the need for a more quantitative understanding of how vegetation and vegetation change influence hydrologic and geomorphic processes, a point also made by Pelletier *et al.* (2015) in the context of improving forecasts of how future climatic and land use changes will impact Earth surface processes.

Cases that do not fit the conceptual model

On soil-mantled hillslopes, soil production and erosion rates are a function of the thickness of soil available for transport (Heimsath *et al.*, 2005), which, in turn, is a function of the long-term difference between erosion and soil production rates, both of which are complex functions of soil temperature, soil moisture, and biological processes controlled by these variables. On weathering-limited hillslopes, soils are generally thin or absent and the erosion rate, by definition, equals the maximum or potential soil production rate because erosion occurs at the same rate that weathering makes soil/debris available for transport. In addition, cliffs are generally devoid of vegetation, hence weathering and transport processes driven by vegetation cover can generally be neglected.

In weathering-limited hillslopes, Burnett *et al.* (2008) documented steeper equator-facing hillslopes with a higher percentage of cliffs compared with pole-facing hillslopes in three canyons incised into the Morrison Formation in northeastern Arizona. Note that this pattern is the opposite of what is typically found in the western USA (i.e. steeper pole-facing hillslopes) but is similar to the Martian mid-latitudes (Kreslavsky and Head, 2003). Using measurements derived from *in situ* soil

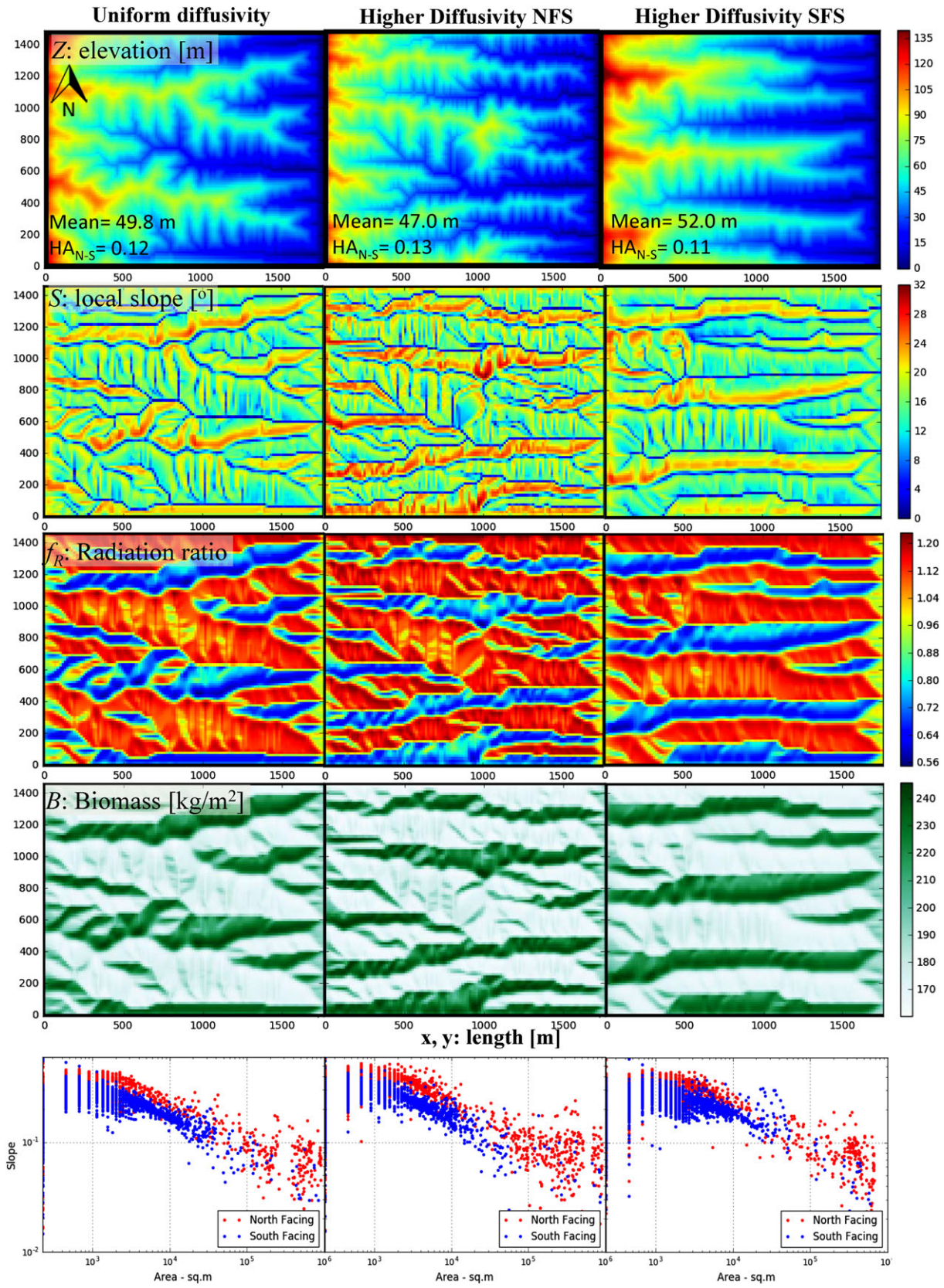

Figure 5. Modeled landscapes computed from a numerical model of ecogeomorphic landform evolution that incorporates insolation as driver of soil moisture dynamics and biomass production (see Appendix A). The domain is 1600 m by 1400 m. The rows show (from top to bottom): elevation (m), radiation ratio, above-ground biomass (kg m^{-2}), and slope angle (degrees). Left column: aspect influences water erosion but not soil creep. Middle column: soil creep efficiency enhanced on pole-facing slopes due to increased vegetation biomass, reflecting enhanced bioturbation. Right column: soil creep efficiency reduced on pole-facing slopes because greater above-ground biomass shields soil from raindrop impact. Note that points with a drainage area greater than 80 000 m^2 generally belong to east-flowing pixels, for which the aspect is poorly defined. Scatter for larger-area points reflects local differences in the sediment influx from surrounding hillslopes. Model was constructed using the Landlab Toolkit (http://landlab.github.io; Hobley *et al.*, 2017) and available as resource on Hydroshare where it can be run using a web browser: https://www.hydroshare.org/resource/6e0cb2146c3e4f2f92ae8a74cb4f3bdd/. Instructions for running the model on Hydroshare can be found in: https://www.hydroshare.org/resource/25040a158eac4730b31eb5ebcc3a7339/. [Colour figure can be viewed at wileyonlinelibrary.com]

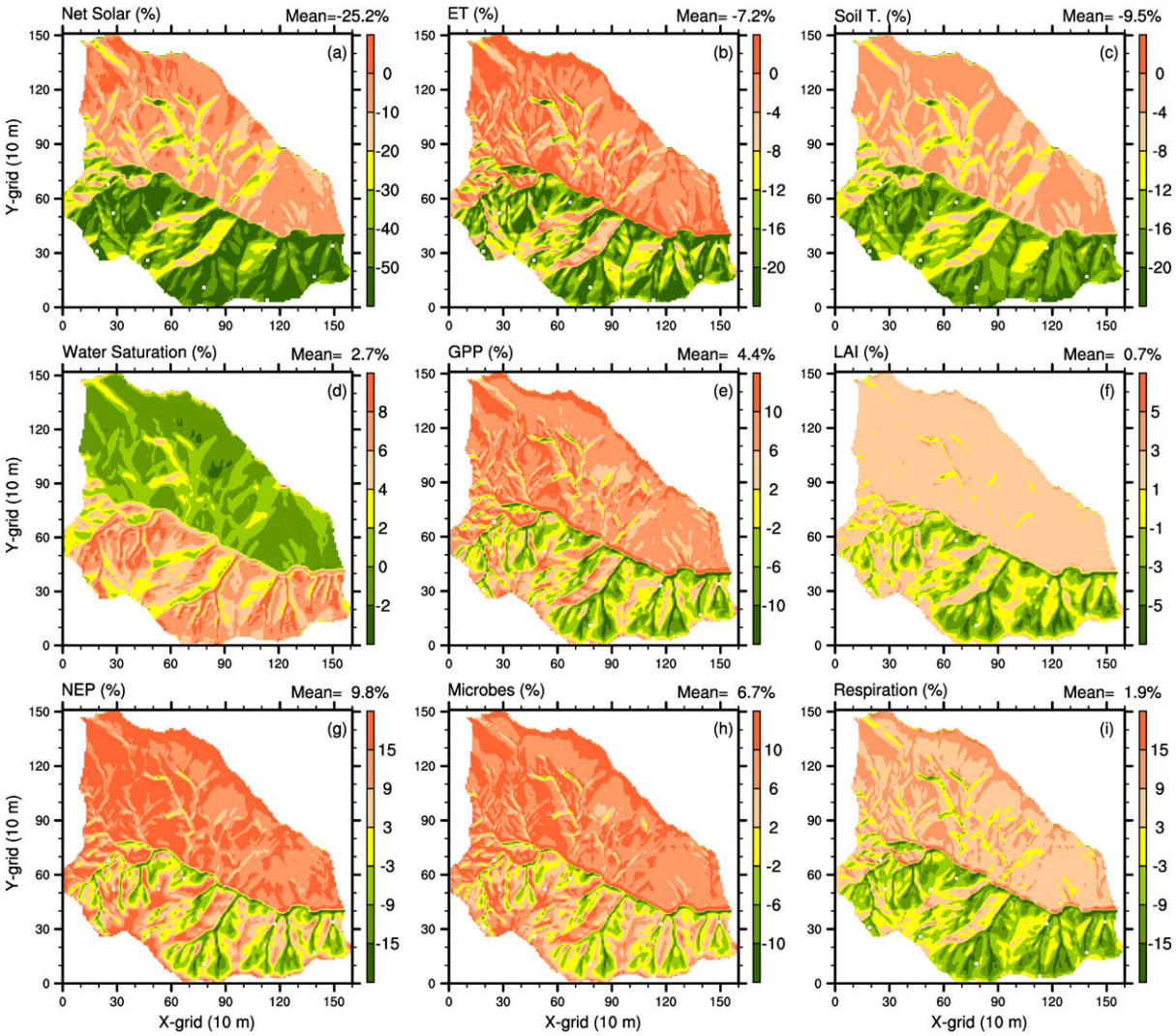

Figure 6. TIMS simulated differences between RADCOR and FLAT. (a) Net solar radiation; (b) ET; (c) soil temperature; (d) degree of water saturation; (e) gross primary productivity (GPP); (f) leaf area index (LAI); (g) net ecosystem productivity (NEP); (h) microbial biomass; and (i) microbial respiration. Shown at the upper-right corner of each panel are the catchment-averaged relative differences (%). [Colour figure can be viewed at wileyonlinelibrary.com]

sensors, Burnett *et al*. (2008) also documented warmer and drier soil conditions on equator-facing hillslopes compared with pole-facing hillslopes. Burnett *et al*. (2008) concluded that more insolation on equator-facing hillslopes results in warmer and drier conditions that inhibit the clay hydration process thought to be the dominant weathering process of the Morrison Formation. Finally, Burnett *et al*. (2008) documented that east-facing hillslopes are more similar to pole-facing hillslopes and west-facing hillslopes more similar to equator-facing hillslopes in terms of the proportion of relief accommodated by cliffs (Burnett *et al*., 2008, Table 5).

At much smaller scales, in the Badlands of South Dakota, Churchill (1982) documented that the south-facing hillslopes of bedrock hoodoos, which lack soil and vegetation cover, were steeper than pole-facing hillslopes. Churchill (1982) found that the pole-facing hillslopes failed more frequently because higher residual moisture content facilitated saturation-induced failures. Similar to Burnett *et al*. (2008), this suggests that bedrock weathering limitations on more arid equator-facing hillslopes produce sediment supply limitations that slow erosion rates. The landform asymmetries observed by both Churchill (1982) and Burnett *et al*. (2008) occur in arid sediment-supply-limited landscapes, which differ fundamentally from the soil-mantled landscape feedbacks focused on in this manuscript. These studies are important for defining the arid end-member conditions of asymmetry found at lower latitudes, and may explain deviations from the modeled results in arid and hyper-arid environments. Additionally, both studies focus on lithologic units that weather by hydration, which suggests that lithology may dictate how landscapes respond to aspect-induced insolation differences.

Non-climatic reasons for asymmetry

The model of this paper invokes climate as the key driver for topographic asymmetry. However, numerous mechanisms that do not rely on microclimate variability have been suggested to explain the presence of topographic asymmetry. Geomorphologists have a long history of investigating topographic asymmetry and have developed many conflicting hypotheses to explain its occurrence. Two ideas that were popular in early literature are that differences in eolian transport due to prevailing winds (Reed, 1927; Bass, 1929; Fairchild, 1932; Emery, 1947) or coriolis forces on stream migration (Gilbert, 1884; Davis, 1895; Fuller, 1914) cause topographic asymmetry, but these explanations have fallen out of favor. However, there are still many reasonable non-climatic explanations for the presence of topographic asymmetry such as faulting, tilted stratigraphy, differences in drainage network competition or initial landscape geometry (Powell, 1874; Bass, 1929; Emery, 1947; Melton, 1960; Dohrenwend, 1978; Wende, 1995).

Sustained lateral channel migration may also produce topographic asymmetry. Differences in sediment deposition at the base of opposing hillslopes drives the main trunk channel across the valley, undercutting and steepening the hillslope. Differences in sediment flux rates may be caused by microclimatic variability (Bass, 1929; Melton, 1960; Dohrenwend, 1978) or natural patterns in the drainage network (Wende, 1995). Although sustained lateral channel migration has been commonly invoked as a possible explanation for the presence of topographic asymmetry (Bass, 1929; Melton, 1960; Dohrenwend, 1978; Istanbulluoglu *et al.*, 2008; García and Mahan, 2009; Poulos *et al.*, 2012), there is limited evidence that lateral channel migration actually produces topographic asymmetry. Johnstone *et al.* (2017), however, documented that certain lithologic types (e.g. mud-rich rocks) may produce profound topographic asymmetry by a set of processes that may include lateral channel migration.

Deciphering whether topographic asymmetry is due to climatic or non-climatic factors is difficult, but important because asymmetry inherently reflects the sensitivity of landscapes to microclimatic variability, and by extension, climate change. Better metrics for determining the specific mechanisms of asymmetry development in different landscapes are needed for understanding microclimate-induced asymmetry. Field measurements of soil properties, topography, and erosion rates may help identify different causes of asymmetry.

Knowledge gaps

The empirical model of this paper (Equation (1)) reproduces the broad-scale patterns of hillslope asymmetry, successfully predicting patterns with latitude and elevation evident in measured hillslope asymmetry maps (Figure 1; Poulos *et al.*, 2012). However, as Figure 3 demonstrates, there are many counterexamples. The sign of asymmetry often reverses across the divides of major mountain ranges in the western USA, changing from steeper pole-facing hillslopes on equator-facing mountain flanks to steeper equator-facing hillslopes on pole-facing mountain flanks (Poulos *et al.*, 2012). Perhaps insolation differences caused by the prevailing mountain-range-scale topography overprint insolation differences caused by local aspect (e.g. insolation is reduced for all slopes, regardless of local aspect, on the poleward side of mountain ranges). However, the proposed water-limited and temperature-limited models could explain this pattern, as equator-facing flanks are more likely to experience water limitations, while the shadier pole-facing flanks of mountain ranges are more likely to be temperature limited. Alternatively, range-scale patterns could be explained by the orientations of the initial land-surfaces on opposite flanks of a mountain range (i.e. a non-climatic cause), as the pattern consistently shows that slopes facing mountain range divides are typically steeper. Higher-resolution models similar to Equation (1) might help explain range-scale asymmetry patterns.

Regional sources of variability unaccounted for by the empirical model might include regional changes in vegetation and biotic communities, lithology and bedrock weathering characteristics, and systematic structural geologic controls. Changes in vegetation communities across regions might introduce variability in slope asymmetry development. Different species of plants have different rooting depths, water needs, canopy cover, litter cover, and stabilizing effects which could influence the processes and rates of erosion, as well as physical and chemical weathering and soil development. Other studies document systematic regional valley asymmetry due to regional tilting (Garrote *et al.*, 2006). Additionally, drainages often form within bedrock fracture networks, inheriting asymmetry from bedrock geometries (Pelletier *et al.*, 2009). If we could identify areas where geologic structure controls landform asymmetry, we might isolate these areas from comparative analyses. Direct assessment of the influence of regional variability in biotic communities, lithology, and bedrock structure might improve our ability to account for them in asymmetry models, or at least constrain analyses to areas where these influences are not prevalent.

Aspect-related landform asymmetry has been studied less at high latitudes (>60°). It is unclear whether the trends exhibited in hillslope asymmetry maps (Poulos *et al.*, 2012) can be extrapolated to higher latitudes. Meiklejohn (1994) found that equator-facing valley sides had gentler slopes on Alexander Island, Antarctica, suggesting that perhaps at extreme latitudes increased insolation on equator-facing hillslopes allows geomorphic action, while pole-facing hillslopes are too cold for even ice to move. A critical step towards unravelling how different asymmetry types develop is to subdivide the landscape into regions, or provinces, where different types of asymmetry prevail.

While there remains a need to better understand how biogeochemical stocks and processes vary in time and space within and between aspects, there is a large gap in our understanding of how short-term biogeochemical processes link to 'deep time', the 'deep' critical zone, or the focus on landscape evolution in CZ science. Do water and reactive constituents make it to the weathering front during pulsed transport events on equator-facing hillslopes? Are there microbes at the weathering front that act on fresh bedrock? How might the relative roles of above-ground vegetative and below-ground microbial activity differentially drive CZ function across topography under projected climate changes that might serve to accentuate or modulate the influence of aspect? These are important questions that link across the disciplines of biogeochemistry, hydrology, and geomorphology, as well as time and space.

The future of the CZ in a warming world: Are equator-facing hillslopes an analog for what pole-facing hillslopes might become?

Projected nonlinear changes to the surface energy budget and water cycle, related to (1) increased MAT, (2) a higher frequency of extreme precipitation events, and (3) rapid shifts in vegetation cover, are likely to alter the rates of landscape evolution differently across all slope aspects. The conceptual model of Figure 4(a) suggests that for water-limited landscapes, warmer temperatures and an increase in extreme rainfall events will trigger positive feedbacks leading to landscape with less vegetation cover, thinner soils, lower soil moisture, and higher erosion rates. Coupled with catastrophic wildfire, these changes could occur in some places over decades rather than centuries; thus, accelerating CZ processes on the landscape.

In regard to (1) increased MAT, the present rate of warming was recently estimated to be 170 times faster than the natural background rate (Gaffney and Steffen, 2017). An 'Anthropocene' shift +5°C to +8°C hotter in the next one hundred to two hundred years will move MAT to a regime not experienced in the last 66 million years (Zeebe *et al.*, 2016). These higher temperatures are likely to differentially accelerate key CZ processes, including rates of soil CO_2 production and loss, shown to be sensitive in montane systems (Stielstra *et al.*, 2015). In fact, Hu *et al.* (2010) found longer growing seasons lead to less C sequestration in high elevation forests that are dominated by snow because of elevated soil CO_2 loss to the atmosphere in these warmer years. In semi-arid regions temperature limited soil mantles may become water limited soil mantles, greatly altering the local water-balance (Knowles *et al.*, 2015).

In regard to (2), there is an expected increase in the frequency of heavy to extreme precipitation events (Kendon *et al.*, 2014; Trenberth *et al.*, 2015). Coupled with an increased magnitude and frequency of disturbances, the number of exceptionally large wildfire events (Abatzoglou and Williams, 2016) will result in increased unstable surface areas being exposed, leading to erosion and landslides. Changes to the timing and quantity of precipitation falling as either rain or snow will also impact catchment scale water budget differently by slope aspect (Brooks *et al.*, 2015).

In regard to (3) anthropogenic climate change is anticipated to cause large-scale die-offs of forests globally in the coming decades (Allen *et al.*, 2015). Many forest ecosystems in complex terrain have taken centuries to millennia to establish their present structure. How will large die off of forest structure influence CZ processes across slope aspect? In terms of physical processes, forest loss from global change type drought or wildfire will feedback to alter surface structure, energy balance, and associated albedo (Villegas *et al.*, 2017). In terms of biological processes, a change in the water budget related to earlier snow-melt (Barnett *et al.*, 2005) on equator facing aspects will impact forests that rely mainly on snow water for metabolic maintenance (respiration) and growth (NPP) processes. Breshears *et al.* (2008) predicted vegetation to synchronously 'lean' upslope as anthropogenic climate change proceeds. Kelly and Goulden (2008) found over a 30-year period the average elevation for species along a 2300 m elevation gradient transect increased by ~65 m a.m.s.l. Given that increased temperature has been shown to increase tree mortality, particularly under drought (McDowell et al., 2016; Adams *et al.*, 2017), we predict that either established forests will die sooner on equator-facing aspects, which can be 5°C warmer than sites on similar elevation pole-facing aspects, or existing vegetation communities currently growing on equator-facing aspects may shift toward pole- facing aspects.

Conclusions

In this paper we reviewed the state of knowledge on slope aspect controls on CZ processes using the latitudinal and elevational dependence of topographic asymmetry as a unifying question. We documented that pole-facing hillslopes tend to be steeper at lower latitudes and elevations, reversing to steeper equator-facing hillslopes at higher latitudes and elevations. We reproduced this pattern at regional to global scales using an empirical model that includes latitude, an aridity index, mean-annual temperature, and mean slope gradient. This model demonstrates the interplay among latitude and relief (which control insolation differences on hillslopes of pole- and equator-facing hillslopes), aridity, and temperature.

We also presented a conceptual model for slope-aspect-driven CZ feedbacks on hillslopes based on water-limited and temperature-limited end-member cases. In water-limited cases, higher mean-annual soil moisture on pole-facing hillslopes generally drive higher soil production rates, higher water storage potential, more vegetation cover, faster dust deposition, and lower erosion rates in a positive feedback. At higher latitudes and elevations, pole-facing hillslopes tend to have less vegetation cover, higher erosion rates, and hence gentler slopes, thus reversing the pattern of topographic asymmetry found at lower latitudes and elevations. Differences in slope gradient and regolith/soil thickness act as both a template for producing slope-aspect differences in ecohydrologic processes and as part of feedback processes that can further drive slope-aspect-driven asymmetry in a wide range of CZ stocks and fluxes.

The models of this paper provide a greater understanding of how topographic asymmetry comes about. We argue that vegetation plays a critical role in driving slope-aspect differences in both end-member cases. We also demonstrate the importance of paleoclimatic conditions and non-climatic factors in influencing slope aspect variations on hillslopes in some cases. Finally, we suggest that steep, equator-facing hillslopes provide a model for the likely directions of change of among CZ stocks and fluxes that will be experienced by hillslopes of gentle slopes and/or pole-facing aspects in a warming world.

Acknowledgements—This study was supported by National Science Foundation Science Across Virtual Institutes Program award #14-45246 and by the following awards of the National Science Foundation Critical Zone program: EAR-1331828, EAR-1331872, and EAR-1331408. In addition, T.L.S. was supported DBI-0735191 and DBI-1265383, G.B.G. was supported by EAR-1417101 and G.E.T. was supported by OAC-1450409. We wish to thank the AE, Samuel Johnstone, and one anonymous reviewer for helpful comments that greatly improved the manuscript.

References

Abatzoglou JT, Williams AP. 2016. Impact of anthropogenic climate change on wildfire across western US forests. *Proceedings of the National Academy of Sciences* **113**(42): 11,770–11,775. https://doi.org/10.1073/pnas.1607171113

Acosta V, Schildgen TF, Clarke BA, Scherler D, Bookhagen B, Wittmann H, von Blanckenburg F, Strecker MR. 2015. Effect of vegetation cover on millennial-scale landscape denudation rates in East Africa. *Lithosphere* **7**(4): 408–420. https://doi.org/10.1130/L402.1

Adams HD et al. 2017. A multi-species synthesis of physiological mechanisms in drought-induced tree mortality. *Nature Ecology & Evolution*. https://doi.org/10.1038/s41559-017-0248-x

Aguilar C, Herrero J, Polo MJ. 2010. Topographic effects on solar radiation distribution in mountainous watersheds and their influence on reference evapotranspiration estimates at watershed scale. *Hydrology and Earth System Sciences* **14**(12): 2479–2494. https://doi.org/10.5194/hess-14-2479-2010

Allen CD, Breshears DD, McDowell NG. 2015. On underestimation of global vulnerability to tree mortality and forest die-off from hotter drought in the Anthropocene. *Ecosphere* **6**(8): 1–55. https://doi.org/10.1890/ES15-00203.1

Anderson RS, Anderson SP, Tucker GE. 2013. Rock damage and regolith transport by frost: an example of climate modulation of the geomorphology of the critical zone. *Earth Surface Processes and Landforms* **38**: 299–316. https://doi.org/10.1002/esp.3330

Anderson SW, Anderson SP, Anderson RS. 2015. Exhumation by debris flows in the 2013 Colorado Front Range storm. *Geology* **43**(5): 391–394. https://doi.org/10.1130/G36507.1

Armesto JJ, Martínez JA. 1978. Relations between vegetation structure and slope aspect in the mediterranean region of Chile. *Journal of Ecology* **66**(3): 881–889. https://doi.org/10.2307/2259301

ASCE-EWRI. 2005. The ASCE Standardized Reference Evapotranspiration Equation. In *Standardization of Reference Evapotranspiration Task Committee Final Report*, Allen RG, Walter IA, Elliot RL, Howell TA, Itenfisu D, Jensen ME, Snyder RL (eds). ASCE Environmental and Water Resources Institute (EWRI): Reston, VA.

Bailey JD, Harrington CA. 2006. Temperature regulation of bud-burst phenology within and among years in a young Douglas-fir (*Pseudotsuga menziesii*) plantation in western Washington, USA. *Tree Physiology* **26**: 421–430. https://doi.org/10.1093/treephys/26.4.421

Bale CL, Williams JB, Charley JL. 1998. The impact of aspect on forest structure and floristics in some Eastern Australian sites. *Forest Ecology and Management* **110**(1-3): 363–377. https://doi.org/10.1016/S0378-1127(98)00300-4

Bandler A. 2016. Geophysical constraints on critical zone architecture and subsurface hydrology of opposing montane hillslopes. Unpublished MS thesis, Colorado School of Mines.

Barnett TP, Adam JC, Lettenmaier DP. 2005. Potential impacts of a warming climate on water availability in snow-dominated regions. *Nature* **438**(7066): 303–309. https://doi.org/10.1038/nature04141

Barron-Gafford GA, Scott RL, Jenerette GD, Huxman TE. 2011. The relative controls of temperature, soil moisture, and plant functional group on soil CO_2 efflux at diel, seasonal, and annual scales. *Journal of Geophysical Research – Biogeosciences* **116**: G01023. https://doi.org/10.1029/2010JG001442

Bass NW. 1929. The Geology of Cowley County, Kansas. *Kansas Geological Survey Bulletin* **12**: 17–23.

Befus KM, Sheehan AF, Leopold M, Anderson SP, Anderson RS. 2011. Seismic constraints on critical zone architecture, Boulder Creek Watershed, Colorado. *Vadose Zone Journal* **10**: 915–927. https://doi.org/10.2136/vzj2010.0108

Begum F, Bajracharya RM, Sharma S, Sitaula BK. 2010. Influence of slope aspect on soil physico-chemical and biological properties in the mid hills of central Nepal. *International Journal of Sustainable Development and World Ecology* **17**(5): 438–443. https://doi.org/10.1080/13504509.2010.499034

Belnap J, Welter JR, Grimm NB, Barger N, Ludwig JA. 2005. Linkages between microbial and hydrologic processes in arid and semiarid watersheds. *Ecology* **86**: 298–307. https://doi.org/10.1890/03-0567

Beudin A, Lakra TS, Ganju KJ, Warner JC. 2017. Development of a coupled wave-flow-vegetation interaction model. *Computers & Geosciences* **100**: 76–86. https://doi.org/10.1016/j.cageo.2016.12.010

Bode CA, Limm MP, Power ME, Finlay JC. 2014. Subcanopy Solar Radiation model: Predicting solar radiation across a heavily vegetated landscape using LiDAR and GIS solar radiation models. *Remote Sensing of Environment* **154**: 387–397. https://doi.org/10.1016/j.rse.2014.01.028

Boyko H. 1947. On the role of plants as quantitative climate indicators and the geo-ecological law of distributions. *Journal of Ecology* **25**: 138–157. https://doi.org/10.2307/2256504

Burnett BN, Meyer GA, McFadden D. 2008. Aspect-related microclimatic influences on slope forms and processes, northeastern Arizona. *Journal of Geophysical Research: Earth Surface* **113**: F03002. https://doi.org/10.1029/2007JF000789

Bradley BA, Mustard JF. 2006. Characterizing the landscape dynamics of an invasive plant and risk of invasion using remote sensing. *Ecological Applications* **16**(3): 1132–1147. https://doi.org/10.1890/1051-0761(2006)016[1132:CTLDOA]2.0.CO;2

Bradstock RA, Hammill KA, Collins L, Price O. 2010. Effects of weather, fuel and terrain on fire severity in topographically diverse landscapes of south-eastern Australia. *Landscape Ecology* **25**(4): 607–619. https://doi.org/10.1007/s10980-009-9443-8

Brantley SL, Eissenstat DM, Marshall JA, Godsey SE, Balogh-Brunstad Z, Karwan DL, Papuga SA, Roering J, Dawson TE, Evaristo J, Chadwick O, McDonnell JJ, Weathers KC. 2017. Reviews and syntheses: On the roles trees play in building and plumbing the Critical Zone. *Biogeosciences Discussions*. https://doi.org/10.5194/bg-2017-2061

Bras RL. 1990. *Hydrology, An Introduction to Hydrologic. Science*, 1st edn. Addison-Wesley Publishing Company: USA.

Breshears DD, Nyhan JW, Heil CE, Wilcox BP. 1998. Effects of woody plants on microclimate in a semiarid woodland: soil temperature and evaporation in canopy and intercanopy patches. *International Journal of Plant Sciences* **159**: 1010–1017. https://doi.org/10.1086/314083

Breshears DD, Huxman TE, Adams HD, Zou CB, Davison JE. 2008. Vegetation synchronously leans upslope as climate warms. *Proceedings of the National Academy of Sciences* **105**(33): 11591–11592. https://doi.org/10.1073/pnas.0806579105

Brooks PD, Chorover J, Fan Y, Godsey SE, Maxwell RM, McNamara JP, Tague C. 2015. Hydrological partitioning in the critical zone: Recent advances and opportunities for developing transferable understanding of water cycle dynamics. *Water Resources Research* **51**: 6973–6987. https://doi.org/10.1002/2015WR017039

Broxton PD, Troch PA, Lyon SW. 2009. On the role of aspect to quantify water transit times in small mountainous catchments. *Water Resources Research* **45**: W08427. https://doi.org/10.1029/2008WR007438

Camporese M, Paniconi C, Putti M, Orlandini S. 2010. Surface-subsurface flow modeling with path-based runoff routing, boundary condition-based coupling, and assimilation of multisource observation data. *Water Resources Research* **46**: W02512. https://doi.org/10.1029/2008WR007536

Carter BJ, Ciolkosz EJ. 1991. Slope gradient and aspect effects on soils developed from sandstone in Pennsylvania. *Geoderma* **49**: 199–213. https://doi.org/10.1016/0016-7061(91)90076-6

Chen XF, Chen JM, An SQ, Ju WM. 2007. Effects of topography on simulated net primary productivity at landscape scale. *Journal of Environmental Management* **85**(3): 585–596. https://doi.org/10.1016/j.jenvman.2006.04.026

Churchill RR. 1982. Aspect-induced differences in hillslope processes. *Earth Surface Processes and Landforms* **7**(2): 171–182. https://doi.org/10.1002/esp.3290070209

Coe JA, Kean JW, Godt JW, Baum RL, Jones ES, Gochis DJ, Anderson GS. 2014. New insights into debris-flow hazards from an extraordinary event in the Colorado Front Range. *GSA Today* **24**: 4–10. https://doi.org/10.1130/GSATG214A.1

Collatz GJ, Ball JT, Grivet C, Berry JA. 1991. Physiological and environmental regulation of stomatal conductance, photosynthesis and transpiration – a model that includes a laminar boundary layer. *Agricultural and Forest Meteorology* **54**(2–4): 107–136. https://doi.org/10.1016/0168-1923(91)90002-8

Collatz GJ, Ribascarbo M, Berry JA. 1992. A coupled photosynthesis–stomatal conductance model for leaves of C4 plants. *Australian Journal of Plant Physiology* **19**: 519–538. https://doi.org/10.1071/PP9920519

Daniels WL, Everett CJ, Zelazny LW. 1987a. Virgin hardwood forest soils of the southern Appalachian Mountains: I. Soil morphology and geomorphology. *Soil Science Society of America Journal* **51**: 722–729. https://doi.org/10.2136/sssaj1987.03615995005100030029x

Daniels WL, Zelazny LW, Everett CJ. 1987b. Virgin hardwood forest soils of the southern Appalachian Mountains: II. Weathering, mineralogy, and chemical properties. *Soil Science Society of America Journal* **51**: 730–738. https://doi.org/10.2136/sssaj1987.03615995005100030030x

Davis WM. 1895. Deflection of rivers by the Earth's rotation: Deflected rivers in Australia. *Science* **27**: 32–33.

Day FP, Monk CD. 1974. Vegetation patterns on a southern Appalachian watershed. *Ecology* **55**(5): 1064–1074. https://doi.org/10.2307/1940356

De Jong J. 1980. *Een karakterisering van de zonnestraling in Nederland*. Dr. Vakgr. Fys. Asp. van Gebouw. Omgeving afd. Bouwkd. en Vakgr. Warmte-en Stromingstechnieken afd. Werktuigbouwkunde, Tech. Hogesch. (Techn. Univ.): Eindhoven, Netherlands.

Deslauriers A, Morin H, Begin Y. 2003. Cellular phenology of annual ring formation of *Abies balsamea* in the Quebec boreal forest (Canada). *Canadian Journal of Forestry Research* **33**: 190–200. https://doi.org/10.1139/x02-178

Desta F, Colbert JJ, Rentch JS, Gottschalk KW. 2004. Aspect induced differences in vegetation, soil, and microclimatic characteristics of an Appalachian watershed. *Castanea* **69**(2): 92–108. https%3A%2F%2Fdoi.org%2F10.2179%2F0008-7475(2004)069%253C0092%3AAIDIVS%253E2.0.CO%3B2

Dickinson RE. 1983. Land surface processes and climate-surface albedos and energy balance. *Advances in Geophysics* **25**: 305–353. https://doi.org/10.1016/S0065-2687(08)60176-4

Dohrenwend JC. 1978. Systematic valley asymmetry in the central California Coast Ranges. *Geological Society of America Bulletin* **89**(6): 891–900. https://doi.org/10.1130/0016-7606(1978)89

Dozier J, Frew J. 1990. Rapid calculation of terrain parameters for radiation modeling from digital elevation data. *IEEE Transactions on Geoscience and Remote Sensing* **28**(5): 963–969. https://doi.org/10.1109/36.58986

Dunne T, Malmon DV, Mudd SM. 2010. A rain splash transport equation assimilating field and laboratory measurements. *Journal of Geophysical Research* **115**: F01001. https://doi.org/10.1029/2009JF001302

Eamus D. 2003. How does ecosystem water balance affect net primary productivity of woody ecosystems? *Functional Plant Biology* **30**(2): 187–205. https://doi.org/10.1071/FP02084

Ebel BA, Rengers FK, Tucker GE. 2015. Aspect-dependent soil saturation and insight into debris-flow initiation during extreme rainfall in the Colorado Front Range. *Geology* **43**(8): 659–662. https://doi.org/10.1130/G36741.1

Eger A, Hewitt AE. 2008. Soils and their relationship to aspect and vegetation history in the eastern Southern Alps, Canterbury High Country, South Island, New Zealand. *Catena* **75**(3): 297–307. https://doi.org/10.1016/j.catena.2008.07.008

Egli M, Mirabella A, Sartori G, Zanelli R, Bischof S. 2006. Effect of north and south exposure on weathering rates and clay mineral formation in Alpine soils. *Catena* **67**(3): 155–174. https://doi.org/10.1016/j.catena.2006.02.010

Egli M, Sofia NL, Kirill C, Svyatoslav I, Yurii P, Dmitry G. 2015. Microclimate affects soil chemical and mineralogical properties of cold alpine soils of the Altai Mountains (Russia). *Journal of Soils and Sediments* **15**: 1420–1436. https://doi.org/10.1007/s11368-013-0838-4

Emery KO. 1947. Asymmetrical valleys of San Diego County, California. *Bulletin of the Southern California Academy of Sciences* **46**(2): 61–71.

Emmingham WH. 1977. Comparison of selected Douglas-fir seed sources for cambial and leader growth patterns in four western Oregon environments. *Canadian Journal of Forestry Research* **7**: 154–164.

Fairchild HL. 1932. Earth rotation and river erosion. *Science* **76**: 423–426. https://doi.org/10.1126/science.76.1976.423

Farquhar GD, von Caemmerer S, Berry JA. 1980. A biochemical model of photosynthetic CO2 assimilation in leaves of C3 species. *Planta* **149**: 78–90. https://doi.org/10.1007/BF00386231

Foster MA, Anderson RS, Wyshnytzky CE, Ouimet WB, Dethier DP. 2015. Using 10Be to deduce rates of landscape evolution and mobile-regolith residence times in Gordon Gulch, Boulder Creek CZO. *Geological Society of America Bulletin* **127**(5/6): 862–878. https://doi.org/10.1130/B31115.1

Fuller ML. 1914. Geology of Long Island. U.S. Geological Survey Professional Paper 252, 50 p.

Gabet EJ, Dunne T. 2002. Landslides on coastal sage-scrub and grassland hillslopes in a severe El Nino winter: The effects of vegetation conversion on sediment delivery. *Geological Society of America Bulletin* **114**(8): 983–990. https%3A%2F%2Fdoi.org%2F10.1130%2F0016-7606(2002)114%253C0983%3ALOCSSA%253E2.0.CO%3B2

Gabet EJ, Dunne T. 2003. Sediment detachment by rain power. *Water Resources Research* **39**: 1002. https://doi.org/10.1029/2001WR000656

Gabet EJ, Reichman OJ, Seabloom EW. 2003. The effects of bioturbation on soil processes and sediment transport. *Annual Review of Earth and Planetary Sciences* **31**(1): 249–273. https://doi.org/10.1146/annurev.earth.31.100901.141314

Gaffney O, Steffen W. 2017. The Anthropocene equation. *The Anthropocene Review*. https://doi.org/10.1177/2053019616688022

García AF, Mahan SA. 2009. Sediment storage and transport in Pancho Rico Valley during and after the Pleistocene-Holocene transition, Coast Ranges of central California (Monterey County). *Earth Surface Processes and Landforms* **34**(8): 1136–1150. https://doi.org/10.1002/esp.1804

Garrote J, Cox RT, Swann C, Ellis M. 2006. Tectonic geomorphology of the southeastern Mississippi Embayment in northern Mississippi, USA. *Geological Society of America Bulletin* **118**(9-10): 1160–1170. https%3A%2F%2Fdoi.org%2F10.1130%2F0091-7613(1980)8%253C442%3A%2520ATOTUS%253E2.0

Geroy IJ, Gribb MM, Marshall HP, Benner SG, McNamara JP, Chandler DG. 2011. Aspect influences on soil water retention and storage. *Hydrological Processes* **25**: 3836–3842. https://doi.org/10.1002/hyp.8281

Gilbert GK. 1884. The sufficiency of terrestrial rotation for the deflection of streams. *American Journal of Science* **27**: 427–432. https://doi.org/10.2475/ajs.s3-27.162.427

Giorgi F. 1988. Dry deposition velocities of atmospheric particles inferred by applying a particle dry deposition parameterization to a general circulation model. *Tellus* **40B**: 23–41. https://doi.org/10.1111/j.1600-0889.1988.tb00210.x

Gustafson JR, Brooks P, Molotch N, Veatch W. 2010. Estimating snow sublimation using natural chemical and isotopic tracers across a gradient of solar radiation. *Water Resources Research* **46**: W12511. https://doi.org/10.1029/2009WR009060

Gutiérrez-Jurado HA, Vivoni ER, Cikoski C, Harrison JBJ, Bras RL, Istanbulluoglu E. 2013. On the observed ecohydrologic dynamics of a semiarid basin with aspect-delimited ecosystems. *Water Resources Research* **49**: 8263–8284. https://doi.org/10.1002/2013WR014364

Hanks TC. 2000. The age of scarplike landforms from diffusion-equation analysis. In *Quaternary Geochronology: Methods and Applications*, Noller JS, Sowers JM, Lettis WR (eds). American Geophysical Union: Washington D.C.; 313–338. https://doi.org/10.1029/RF004p0313

Hargreaves GH, Samani ZA. 1985. Reference crop evapotranspiration from temperature. *Applied Engineering in Agriculture* **1**: 95–99. https://doi.org/10.13031/2013.26773

Harpold AA. 2016. Diverging sensitivity of soil water stress to changing snowmelt timing in the western U.S. *Advances in Water Resources* **92**: 116–129. https://doi.org/10.1016/j.advwatres.2016.03.017

Harpold AA, Molotch NP, Musselman KN, Bales RC, Kirchner PB, Litvak M, Brooks PD. 2014. Soil moisture response to snowmelt timing in mixed-conifer subalpine forests. *Hydrological Processes* **29**(12): 2782–2798. https://doi.org/10.1002/hyp.10400

Heimsath AM, Furbish DJ, Dietrich WE. 2005. The illusion of diffusion: Field evidence for depth dependent sediment transport. *Geology* **33**: 949–952. https://doi.org/10.1130/G21868.1

Heyerdahl EK, Brubaker LB, Agee JK. 2001. Spatial controls of historical fire regimes: A multiscale example from the interior west, USA. *Ecology* **82**(3): 660–678. https%3A%2F%2Fdoi.org%2F10.1890%2F0012-9658(2001)082%255B0660%3ASCOHFR%255D2.0.CO

Hinckley E-LS, Barnes RT, Anderson SP, Williams MW, Bernasconi SM. 2014a. Nitrogen retention and transport differ by hillslope aspect at the rain-snow transition of the Colorado Front Range. *Journal of Geophysical Research – Biogeosciences* **119**(7): 1281–1296. https://doi.org/10.1002/2013JG002588

Hinckley E-LS, Ebel BA, Barnes RT, Anderson RS, Williams MW, Anderson SP. 2014b. Aspect control of water movement on hillslopes near the rain-snow transition of the Colorado Front Range. *Hydrological Processes* **28**(1): 74–85. https://doi.org/10.1002/hyp.9549

Hinckley E-LS, Ebel BA, Barnes RT, Murphy SF, Anderson SP. 2017. Critical zone properties control the fate of nitrogen during experimental rainfall in montane forests of the Colorado Front Range. *Biogeochemistry* **132**(1-2): 213–231. https://doi.org/10.1007/s10533-017-0299-8

Hobley DEJ, Adams JM, Nudurupati SS, Hutton EWH, Gasparini NM, Istanbulluoglu E, Tucker GE. 2017. Creative computing with Landlab: an open-source toolkit for building, coupling, and exploring two-dimensional numerical models of Earth-surface dynamics. *Earth Surface Dynamics* **5**: 21–46. https://doi.org/10.5194/esurf-5-21-2017

Holbrook WS, Riebe CS, Elwaseif M, Hayes JL, Basler-Reeder K, Harry DL, Malazian A, Dosseto A, Hartsough CP, Hopmans WJ. 2014. Geophysical constraints on deep weathering and water storage potential in the Southern Sierra Critical Zone Observatory. *Earth Surface Processes and Landforms* **39**: 366–380. https://doi.org/10.1002/esp.3502

Holland PG, Steyn DG. 1975. Vegetational responses to latitudinal variations in slope angle and aspect. *Journal of Biogeography* **2**: 179–183. https://doi.org/10.2307/3037989

Howard AD. 1994. A detachment-limited model of drainage basin evolution. *Water Resources Research* **30**(7): 2261–2285. https://doi.org/10.1029/94WR00757

Hu J, Moore DJ, Burns SP, Monson RK. 2010. Longer growing seasons lead to less carbon sequestration by a subalpine forest. *Global Change Biology* **16**(2): 771–783. https://doi.org/10.1111/j.1365-2486.2009.01967.x

Hughes M, Almond P, Roering J. 2009. Increased sediment transport via bioturbation at the last glacial-interglacial transition. *Geology* **37**: 919–922. https://doi.org/10.1130/G30159A.1

Hunckler RV, Schaetzl RJ. 1997. Spodosol development as affected by geomorphic aspect, Baraga County, Michigan. *Soil Science Society of America Journal* **61**: 1105–1115. https://doi.org/10.2136/sssaj1997.03615995006100040017x

Hurst MD, Mudd SM, Attal M, Hilley G. 2013. Hillslopes record the growth and decay of landscapes. *Science* **341**: 868. https://doi.org/10.1126/science.1241791

Hutchins RB, Blevins RL, Hill JD, White EH. 1976. The influence of soils and microclimate on vegetation of forested slopes in eastern Kentucky. *Soil Science* **121**: 234–241. https://doi.org/10.1097/00010694-197604000-00008

Inbar M, Wittenberg L, Tamir M. 1997. Soil erosion and forestry management after wildfire in a Mediterranean woodland, Mt. Carmel, Israel. *International Journal of Wildland Fire* **7**(4): 285–294. https://doi.org/10.1071/WF9970285

Irmak S, Istanbulluoglu E, Irmak A. 2008. An evaluation of evapotranspiration model complexity against performance in comparison with Bowen Ratio Energy Balance latent heat measurements. *Transactions of the American Society of Agricultural and Biological Engineers* **51**(4): 1295–1310.

Istanbulluoglu E, Bras RL. 2005. Vegetation-modulated landscape evolution: Effects of vegetation on landscape processes, drainage density, and topography. *Journal of Geophysical Research* **110**: F02012. https://doi.org/10.1029/2004JF000249

Istanbulluoglu E, Yetemen O, Vivoni ER, Gutiérrez-Jurado HA, Bras RL. 2008. Eco-geomorphic implications of hillslope aspect: Inferences from analysis of landscape morphology in central New Mexico. *Geophysical Research Letters* **35**: L14403. https://doi.org/10.1029/2008GL034477

Jackson M, Roering JJ. 2009. Post-fire geomorphic response in steep, forested landscapes: Oregon Coast Range, USA. *Quaternary Science*

Reviews **28**(11): 1131–1146. https://doi.org/10.1016/j.quascirev.2008.05.003
Jarvis A, Reuter HI, Nelson A, Guevara E. 2008. Hole-filled SRTM for the globe Version 4. Digital Data available from http://srtm.csi.cgiar.org
Johnstone SA, Hilley GE. 2015. Lithologic control on the form of soil-mantled hillslopes. *Geology* **43**(1): 83–86. https%3A%2F%2Fdoi.org%2F10.1130%2F0091-761M3(2001)029%253C0683%3ASTMOSM%253E2.0
Johnstone SA, Chadwick KD, Frias M, Tagliaro G, Hilley GE. 2017. Soil development over mud-rich rocks produces landscape-scale erosional instabilities in the northern Gabilon Mesa, California. *Geological Society of America Bulletin*. https://doi.org/10.1130/B31546.1
Kang S, Doh S, Lee D, Lee D, Jin VL, Kimball JS. 2003. Topographic and climatic controls on soil respiration in six temperate mixed-hardwood forest slopes, Korea. *Global Change Biology* **9**(10): 1427–1437. https://doi.org/10.1046/j.1365-2486.2003.00668.x
Kelly AE, Goulden ML. 2008. Rapid shifts in plant distribution with recent climate change. *Proceedings of the National Academy of Sciences of the United States of America* **105**: 11823–11826. https://doi.org/10.1073/pnas.0802891105
Kendon EJ, Roberts NM, Fowler HJ, Roberts MJ, Chan SC, Senior CA. 2014. Heavier summer downpours with climate change revealed by weather forecast resolution model. *Nature Climate Change* **4**(7): 570–576. https://doi.org/10.1038/NCLIMATE2258
Knowles JF, Harpold AA, Cowie R, Zeliff M, Barnard HR, Burns SP, Blanken PD, Morse JF, Williams MW. 2015. The relative contributions of alpine and subalpine ecosystems to the water balance of a mountainous, headwater catchment. *Hydrological Processes* **22**: 4794–4808. https://doi.org/10.1002/hyp.10526
Kreslavsky MA, Head JW. 2003. North-south topographic slope asymmetry on Mars: Evidence for insolation-related erosion at high obliquity. *Geophysical Research Letters* **30**: 1815. https://doi.org/10.1029/2003GL017795
Kunkel ML, Flores AN, Smith TJ, McNamara JP, Benner SG. 2011. A simplified approach for estimating soil carbon and nitrogen stocks in semi-arid complex terrain. *Geoderma* **165**: 1–11. https://doi.org/10.1016/j.geoderma.2011.06.011
Kutiel P. 1992. Slope aspect effect on soil and vegetation in a Mediterranean ecosystem. *Israel Journal of Botany* **41**(4-6): 243–250. https://doi.org/10.1080/0021213X.1992.10677231
Kutiel P, Lavee H. 1999. Effect of slope aspect on soil and vegetation properties along an aridity transect. *Israel Journal of Plant Sciences* **47**(3): 169–178. https://doi.org/10.1080/07929978.1999.10676770
Laio F, Porporato A, Ridolfi L, Rodriguez-Iturbe I. 2001. Plants in water-controlled ecosystems: active role in hydrologic processes and response to water stress II. Probabilistic soil moisture dynamics. *Advances in Water Resources* **24**: 707–723. https://doi.org/10.1016/S0309-1708(01)00004-5
Langston AL, Tucker GE, Anderson RS, Anderson SP. 2015. Evidence for climatic and hillslope-aspect controls on vadose zone hydrology and implications for saprolite weathering. *Earth Surface Processes and Landforms* **40**(9): 1254–1269. https://doi.org/10.1002/esp.3718
Le Bouteiller C, Venditti JG. 2015. Sediment transport and shear stress partitioning in a vegetated flow. *Water Resources Research* **51**: 2901–2922. https://doi.org/10.1002/2014WR015825
Lebedeva MI, Brantley SL. 2013. Exploring geochemical controls on weathering and erosion of convex hillslopes: beyond the empirical regolith production function. *Earth Surface Processes and Landforms* **38**: 1793–1807. https://doi.org/10.1002/esp.3424
Losche CK, McCracken RJ, Davey CB. 1970. Soils of steeply sloping landscapes in the southern Appalachian Mountains. *Proceedings of the Soil Science Society of America* **34**(3): 473–478. https://doi.org/10.2136/sssaj1970.03615995003400030033x
Lybrand R, Rasmussen C, Jardine A, Troch PA, Chorover J. 2011. The effects of climate and landscape position on chemical denudation and mineral transformation in the Santa Catalina mountain critical zone observatory. *Applied Geochemistry* **26**(S): S80–S84. https://doi.org/10.1016/j.apgeochem.2011.03.036
Macyk TM, Lindsay JD, Pawluk S. 1978. Relief and microclimate as related to soil properties. *Canadian Journal of Soil Science* **58**: 421–438. https://doi.org/10.4141/cjss78-049
Mahowald N, Kohfeld K, Hansson M, Balkanski Y, Harrison SP, Prentice IC, Schulz M, Rodhe H. 1999. Dust sources and deposition during the last glacial maximum and current climate: A comparison of model results with paleodata from ice cores and marine sediments. *Journal of Geophysical Research* **104**(D13): 15,895–15,916. https://doi.org/10.1029/1999JD900084
Marin CT, Bouten W, Sevink J. 2000. Gross rainfall and its partitioning into throughfall, stemflow and evaporation of intercepted water in four forest ecosystems in western Amazonia. *Journal of Hydrology* **237**(1): 40–57. https://doi.org/10.1016/S0022-1694(00)00301-2
Martin Y. 2000. Modelling hillslope evolution: linear and nonlinear transport relations. *Geomorphology* **34**: 1–21. https://doi.org/10.1016/S0169-555X(99)00127-0
Mascaro G, Vivoni ER. 2016. On the observed hysteresis in field-scale soil moisture variability and its physical controls. *Environmental Research Letters* **11**: 0840008. https://doi.org/10.1088/1748-9326/11/8/084008
McClain ME, Boyer EW, Dent CL, Gergel SE, Grimm NB, Groffman PM, Hart SC, Harvey JW, Johnston CA, Mayorga E, McDowell WH, Pinay G. 2003. Biogeochemical Hot Spots and Hot Moments at the Interface of Terrestrial and Aquatic Ecosystems. *Ecosystems* **6**: 301–312. https://doi.org/10.1007/s10021-003-0161-9
McDowell NG, Williams AP, Xu C, Pockman WT, Dickman LT, Sevanto S, Pangle R, Limousin J, Plaut J, Mackay DS et al. 2016. Multi-scale predictions of massive conifer mortality due to chronic temperature rise. *Nature Climate Change* **6**(3): 295–300. https://doi.org/10.1038/nclimate2873
McGuire LA, Pelletier JD, Roering JJ. 2014. Development of topographic asymmetry: Insights from dated cinder cones in the western United States. *Journal of Geophysical Research – Earth Surface* **119**: 1725–1750. https://doi.org/10.1002/2014JF003081
McGuire LA, Rengers FK, Kean JW, Coe JA, Mirus BB, Baum RL, Godt JW. 2016. Elucidating the role of vegetation in the initiation of rainfall-induced shallow landslides: Insights from an extreme rainfall event in the Colorado Front Range. *Geophysical Research Letters* **43**(17): 9084–9092. https://doi.org/10.1002/2016GL070741
Meiklejohn KI. 1994. Valley asymmetry on south-eastern Alexander Island, Antarctica, and valley forms in the high Drakensberg, southern Africa. *South African Geographical Journal* **76**(2): 68–72. https://doi.org/10.1080/03736245.1994.9713578
Melton MA. 1960. Intravalley Variation in Slope Angles Related to Microclimate and Erosional Environment. *Geological Society of America Bulletin* **71**: 133–144. https://doi.org/0.1130/0016-7606(1960)71[133:IVISAR]2.0.CO;2
Molotch NP, Brooks PD, Burns SP, Litvak M, Monson RK, McConnell JR, Musselman K. 2009. Ecohydrological controls on snowmelt partitioning in mixed-conifer sub-alpine forests. *Ecohydrology* **2**: 129–142. https://doi.org/10.1002/eco.48
Moody JA, Ebel BA, Nyman P, Martin DA, Stoof C, McKinley R. 2016. Relations between soil hydraulic properties and burn severity. *International Journal of Wildland Fire* **25**(3): 279–293. https://doi.org/10.1071/WF14062
Nepf HM. 2012. Flow and transport in regions with aquatic vegetation. *Annual Review of Fluid Mechanics* **44**: 123–142. https://doi.org/10.1146/annurev-fluid-120710-101048
Niu G-Y, Yang Z-L. 2004. Effects of vegetation canopy processes on snow surface energy and mass balances. *Journal of Geophysical Research* **109**: D23111. https://doi.org/10.1029/2004JD004884
Niu G-Y, Yang Z-L, Mitchell KE, Chen F, Ek MB, Barlage M, Kumar A, Manning K, Niyogi D, Rosero E, Tewari M, Xia Y. 2011. The community Noah land surface model with multiparameterization options (Noah-MP): 1. Model description and evaluation with local-scale measurements. *Journal of Geophysical Research* **16**: D12109. https://doi.org/10.1029/2010JD015139
Niu G-Y, Paniconi C, Troch PA, Scott RL, Durcik M, Zeng X, Huxman T, Goodrich DC. 2014. An integrated modelling framework of catchment-scale ecohydrological processes: 1. Model description and tests over an energy-limited watershed. *Ecohydrology* **7**(2): 427–439. https://doi.org/10.1002/eco.1362
Olyphant J, Pelletier JD, Johnson R. 2016. Topographic correlations with soil and regolith thickness from shallow-seismic refraction constraints across upland hillslopes in the Valles Caldera, New Mexico. *Earth Surface Processes and Landforms* **41**: 1684–1696. https://doi.org/10.1002/esp.3941
Orem CA, Pelletier JD. 2016. The predominance of post-wildfire erosion in the long-term denudation of the Valles Caldera, New Mexico. *Journal of Geophysical Research – Earth Surface* **121**: 843–864. https://doi.org/10.1002/2015JF003663
Pelletier JD, Orem CA. 2014. How do sediment yields from post-wildfire debris-laden flows depend on terrain slope, soil burn severity

class, and drainage basin area? Insights from airborne-lidar change detection. *Earth Surface Processes and Landforms* **39**(13): 1822–1832. https://doi.org/10.1002/esp.3570

Pelletier JD, Rasmussen C. 2009. Quantifying the climatic and tectonic controls on hillslope steepness and erosion rates. *Lithosphere* **1**: 73–80. https://doi.org/10.1130/L3.1

Pelletier JD, Swetnam TL. 2017. Asymmetry of weathering-limited hillslopes: The importance of diurnal covariation in insolation and temperature. *Earth Surface Processes and Landforms*. https://doi.org/10.1002/esp.4136

Pelletier JD, Engelder TM, Comeau D, Hudson A, Leclerc M, Youberg A, Diniega S. 2009. Tectonic and structural control of fluvial channel morphology in metamorphic core complexes: The example of the Catalina-Rincon core complex, Arizona. *Geosphere* **5**: 363–384. https://doi.org/10.1130/GES00221.1

Pelletier JD, McGuire LA, Ash JL, Engelder TM, Hill LE, Leroy KW, Orem CA, Rosenthal WS, Trees MA, Rasmussen C, Chorover J. 2011. Calibration and testing of upland hillslope evolution models in a dated landscape: Banco Bonito, New Mexico. *Journal of Geophysical Research* **116**: F04004. https://doi.org/10.1029/2011JF001976

Pelletier JD, Barron-Gafford GA, Breshears DD, Brooks PD, Chorover J, Durcik M, Harman CJ, Huxman TE, Lohse KA, Lybrand R, Meixner T, McIntosh JC, Papuga SA, Rasmussen C, Schaap M, Swetnam TL, Troch PA. 2013. Coevolution of nonlinear trends in vegetation, soils, and topography with elevation and slope aspect: A case study in the sky islands of southern Arizona. *Journal of Geophysical Research – Earth Surface* **118**(2): 741–758. https://doi.org/10.1029/2012JF002569

Pelletier JD, Murray AB, Pierce JL, Bierman PR, Breshears DD, Crosby BT, Ellis M, Foufoula-Georgiou E, Heimsath AM, Houser C, Lancaster N, Marani M, Merritts DJ, Moore LJ, Pederson JL, Poulos MJ, Rittenour TM, Rowland JC, Ruggiero P, Ward DJ, Wickert AD, Yager EM. 2015. Forecasting the response of Earth's surface to future climatic and land use changes: A review of methods and research needs. *Earth's Future* **3**: 220–251. https://doi.org/10.1002/2014EF000290

Perring F. 1959. Topographical gradients of chalk grassland. *Journal of Ecology* **47**: 447–481. https://doi.org/10.2307/2257376

Perron JT, Dietrich WE, Kirchner JE. 2008. Controls on the spacing of first-order valleys. *Journal of Geophysical Research – Earth Surface* **113**: F04016. https://doi.org/10.1029/2007jf000977

Pomeroy JW, Parviainen J, Hedstrom N, Gray DM. 1998. Coupled modelling of forest snow interception and sublimation. *Hydrological Processes* **12**(15): 2317–2337. https%3A%2F%2Fdoi.org%2F10.1002%2F(SICI)1099-1085(199812)12%3A15%253C2317%3A%3AAID-HYP799%253E3.0

Porporato A, Laio F, Ridolfi L, Rodriguez-Iturbe I. 2001. Plants in water controlled ecosystems: Active role in hydrologic processes and response to water stress III. Vegetation water stress. *Advances in Water Resources* **24**: 725–744. https://doi.org/10.1016/S0309-1708(01)00006-9

Porporato A, Daly E, Rodriguez-Iturbe I. 2004. Soil water balance and ecosystem response to climate change. *American Naturalist* **164**(5): 625–632. https://doi.org/10.1086/424970

Poulos MJ, Pierce JL, Flores AN, Benner SG. 2012. Hillslope asymmetry maps reveal widespread, multi-scale organization. *Geophysical Research Letters* **39**: L06406. https://doi.org/10.1029/2012GL051283

Powell JW. 1874. Remarks on the structural geology of the valley of the Colorado of the West. *Bulletin of the Washington Philosophical Society* **1**: 48–51.

Quijano JC, Kumar P. 2015. Numerical simulations of hydraulic redistribution across climates: The role of the root hydraulic conductivities. *Water Resources Research* **51**: 8529–8550. https://doi.org/10.1002/2014WR016509

Radcliffe JE, Lefevre KR. 1981. Aspect influences on pasture microclimate at Coopers Creek, North-Canterbury, New Zealand. *Journal of Agricultural Research* **24**: 55–66.

Rasmussen C, Pelletier JD, Troch PA, Swetnam TL, Chorover J. 2015. Quantifying Topographic and Vegetation Effects on the Transfer of Energy and Mass to the Critical Zone. *Vadose Zone Journal* **14**(11). https://doi.org/10.2136/vzj2014.07.0102

Reed RD. 1927. Wind and soil in the Gabilan Mesa. *Journal of Geology* **35**: 84–88. https://doi.org/10.1086/623384

Rempe DM, Dietrich WE. 2014. A bottom-up control on fresh-bedrock topography under landscapes. *Proceedings of the National Academy of Sciences* **111**: 6576–6581. https://doi.org/10.1073/pnas.1404763111

Rengers FK, McGuire LA, Coe JA, Kean JW, Baum RL, Staley DM, Godt JW. 2016. The influence of vegetation on debris-flow initiation during extreme rainfall in the northern Colorado Front Range. *Geology* **44**(10): 823–826. https://doi.org/10.1130/G38096.1

Richardson, PW. 2015. Topographic asymmetry and climate controls on landscape evolution. Ph.D. Dissertation, Massachusetts Institute of Technology. Digital document available at http://hdl.handle.net/1721.1/101346

Roering JJ. 2004. Soil creep and convex-upward velocity profiles: Theoretical and experimental investigation of disturbance-driven sediment transport on hillslopes. *Earth Surface Processes and Landforms* **29**: 1597–1612. https://doi.org/10.1002/esp.1112

Roering JJ. 2008. How well can hillslope evolution models "explain" topography? Simulating soil transport and production with high-resolution topographic data. *Geological Society of America Bulletin* **120**: 1248–1262. https://doi.org/10.1130/B26283.1

Rossi S, Deslauriers A, Anfodillo T, Carraro V. 2007. Evidence of threshold temperatures for xylogenesis in conifers at high altitudes. *Ecophysiology* **152**: 1–12. https://doi.org/10.1007/s00442-006-0625-7

Schmidt KM, Roering JJ, Stock JD, Dietrich WE, Montgomery DR, Schaub T. 2001. The variability of root cohesion as an influence on shallow landslide susceptibility in the Oregon Coast Range. *Canadian Geotechnical Journal* **38**(5): 995–1024. https://doi.org/10.1139/cgj-38-5-995

Schönenberger W, Frey W. 1988. Untersuchungen zur Ökologie und Technik der Hochlagenaufforstung. Forschungsergebnisse aus dem Lawinenanrissgebiet Stillberg. *Schweizerische Zeitschrift für Forstwesen* **139**: 735–820.

Shakesby RA, Doerr SH. 2006. Wildfire as a hydrological and geomorphological agent. *Earth-Science Reviews* **74**(3): 269–307. https://doi.org/10.1016/j.earscirev.2005.10.006

Smith TJ, McNamara JP, Flores AN, Gribb MM, Aishlin PS, Benner SG. 2011. Small soil storage capacity limits benefit of winter snowpack to upland vegetation. *Hydrological Processes* **25**: 3858–3865. https://doi.org/10.1002/hyp.8340

St. Clair J, Moon S, Holbrook WS, Perron JT, Riebe CS, Martel SJ, Carr B, Harman C, Singha K. 2015. Geophysical imaging reveals topographic stress control of bedrock weathering. *Science* **350**(6260): 534–538. https://doi.org/10.1126/science.aab2210

Stephenson NL. 1990. Climatic control of vegetation distribution: The role of the water balance. *American Naturalist* **135**(5): 649–670. https://doi.org/10.1086/285067

Stielstra CM, Lohse KA, Chorover J, McIntosh JC, Barron-Gafford GA, Perdrial JN, Litvak M, Barnard H, Brooks PD. 2015. Climatic and landscape influences on soil moisture are primary determinants of soil carbon fluxes in seasonally snow-covered forest ecosystems. *Biogeochemistry* **123**(3): 447–465. https://doi.org/10.1007/s10533-015-0078-3

Swetnam TW, Betancourt JL. 1998. Mesoscale disturbance and ecological response to decadal climatic variability in the American Southwest. *Journal of Climate* **11**(12): 3128–3147. https%3A%2F%2Fdoi.org%2F10.1175%2F1520-0442(1998)011%253C3128%3AMDAERT%253E2.0.CO%3B2

Tague C, Peng H. 2013. The sensitivity of forest water use to the timing of precipitation and snowmelt recharge in the California Sierra: Implications for a warming climate. *Journal of Geophysical Research – Biogeosciences* **118**(2): 875–887. https://doi.org/10.1002/jgrg.20073

Tarboton DG. 1992. A physical basis for drainage density. *Geomorphology* **5**: 59–76. https://doi.org/10.1016/0169-555X(92)90058-V

Taylor AH, Skinner CN. 1998. Fire history and landscape dynamics in a late-successional reserve, Klamath Mountains, California, USA. *Forest Ecology and Management* **111**(2): 285–301. https://doi.org/10.1016/S0378-1127(98)00342-9

Thompson RS, Whitlock C, Bartlein P, Harrison S, Spaulding W. 1993. Climatic changes in the western United States since 18,000 yr B.P. In *Global Climates Since the Last Glacial Maximum*, Wright H, Jr, Kutzbach J, Webb T, Ruddiman III WR, Street-Perrott F, Bartlein P (eds). University of Minnesota Press; 468–513.

Trenberth KE, Fasullo JT, Shepherd TG. 2015. Attribution of climate extreme events. *Nature Climate Change* **5**: 725–730. https://doi.org/10.1038/nclimate2657

Tucker GE, Whipple KX. 2002. Topographic outcomes predicted by stream erosion models: Sensitivity analysis and intermodel comparison. *Journal of Geophysical Research* **107**(B9): 2179. https://doi.org/10.1029/2001JB000162

Van Devender TR, Dimmitt MA. 2006. Final Report on Conservation of Arizona Upland Sonoran Desert Habitat. Status and Threats of

Buffelgrass (Pennisetum ciliare) in Arizona and Sonora. Project# 2004-0013-003. Arizona-Sonora Desert Museum Tucson, AZ.
Villegas JC, Law DJ, Stark SC, Minor DM, Breshears DD, Saleska SR, Swann ALS, Garcia ES, Bella EM, Morton JM et al. 2017. Prototype campaign assessment of disturbance-induced tree loss effects on surface properties for atmospheric modeling. *Ecosphere* **8**(3). https://doi.org/10.1002/ecs2.1698
Webb WL, Szarek SR, Lauenroth WK, Kinerson RS. 1978. Primary productivity and water use in native forest, grassland, and desert ecosystems. *Ecology* **59**(6): 1239–1247. https://doi.org/10.2307/1938237.
Wende R. 1995. Drainage and valley asymmetry in the Tertiary Hills of Lower Bavaria, Germany. *Geomorphology* **14**: 255–265. https://doi.org/10.1016/0169-555X(95)00114-K
West N, Kirby E, Bierman PA, Clarke BA. 2014. Aspect-dependent variations in regolith creep revealed by meteoric 10Be. *Geology* **42**: 507–510. https://doi.org/10.1130/G35357.1
Whittaker RH, Niering WA. 1965. Vegetation of the Santa Catalina Mountains, Arizona: A gradient analysis of the south slope. *Ecology* **46**(4): 429–452. https://doi.org/10.2307/1934875
Whittaker RH, Niering WA. 1975. Vegetation of the Santa Catalina Mountains, Arizona. V. Biomass, production, and diversity along the elevation gradient. *Ecology* **56**(4): 771–790. https://doi.org/10.2307/1936291
Whittaker RH, Buol SW, Niering WA, Havens YH. 1968. A soil and vegetation pattern in the Santa Catalina Mountains, Arizona. *Soil Science* **105**(6): 440–450. https://doi.org/10.1007/BF00044893
Winchell EW, Anderson RS, Lombardi EM, Doak DF. 2016. Gophers as geomorphic agents in the Colorado Front Range subalpine zone. *Geomorphology* **264**: 41–51. https://doi.org/10.1016/j.geomorph.2016.04.003
Wood SW, Murphy BP, Bowman DM. 2011. Firescape ecology: how topography determines the contrasting distribution of fire and rain forest in the south-west of the Tasmanian Wilderness World Heritage Area. *Journal of Biogeography* **38**(9): 1807–1820. https://doi.org/10.1111/j.1365-2699.2011.02524.x
Yetemen O, Istanbulluoglu E, Vivoni ER. 2010. The implications of geology, soils, and vegetation on landscape morphology: Inferences from semi-arid basins with complex vegetation patterns in Central New Mexico, USA. *Geomorphology* **116**: 246–263. https://doi.org/10.1016/j.geomorph.2009.11.026
Yetemen O, Istanbulluoglu E, Flores-Cervantes JH, Vivoni ER, Bras RL. 2015a. Ecohydrologic role of solar radiation on landscape evolution. *Water Resources Research* **51**: 1127–1157. https://doi.org/10.1002/2014WR016169
Yetemen O, Istanbulluoglu E, Duvall A. 2015b. Solar radiation as a global driver of hillslope asymmetry. *Water Resources Research* **51**: 9843–9861. https://doi.org/10.1002/%202015WR017103
Yoo K, Amundson R, Heimsath AM, Dietrich WE. 2005. Process-based model linking pocket gopher (*Thomomys bottae*) activity to sediment transport and soil thickness. *Geology* **33**(11): 917–920. https://doi.org/10.1130/G21831.1
Zapata-Rios X, Brooks PD, Troch PA, McIntosh J, Guo Q. 2015a. Influence of terrain aspect on water partitioning, vegetation structure and vegetation greening in high-elevation catchments in northern New Mexico. *Ecohydrology* **9**: 782–795. https://doi.org/10.1002/eco.1674
Zapata-Rios X, McIntosh J, Rademacher L, Troch PA, Brooks PD, Rasmussen C, Chorover J. 2015b. Climatic and landscape controls on water transit times and silicate mineral weathering in the critical zone. *Water Resources Research* **51**: 6036–6051. https://doi.org/10.1002/2015WR017018
Zeebe RE, Ridgwell A, Zachos JC. 2016. Anthropogenic carbon release rate unprecedented during the past 66 million years. *Nature Geoscience* **9**(4): 325–329. https://doi.org/10.1038/ngeo2681
Zhang X, Niu G-Y, Elshall AS, Ye M, Barron-Gafford GA, Pavao Zuckerman M. 2014. Assessing five evolving microbial enzyme models against field measurements from a semiarid savannah —What are the mechanisms of soil respiration pulses? *Geophysical Research Letters* **41**: 6428–6434. https://doi.org/10.1002/2014GL061399
Zomer RJ, Trabucco A, Bossio DA, van Straaten O, Verchot LV. 2008. Climate Change Mitigation: A Spatial Analysis of Global Land Suitability for Clean Development Mechanism Afforestation and Reforestation. *Agriculture, Ecosystems and Environment* **126**: 67–80. https://doi.org/10.1016/j.agee.2008.01.014
Zou CB, Barron-Gafford GA, Breshears DD. 2007. Effects of topography and woody plant canopy cover on near-ground solar radiation: Relevant energy inputs for ecohydrology and hydropedology. *Geophysical Research Letters* **34**: L24S21. https://doi.org/10.1029/2007GL031484

Appendix A: Numerical modeling of long-term development of the CZ using Landlab

The conceptual model illustrated in Figure 3 constitutes a general hypothesis for the origin of aspect-related terrain asymmetry. To place this hypothesis in a quantitative, mechanistic framework, it is useful to test whether models that embody a given subset of the feedbacks illustrated in Figure 4 can successfully account for the observed topographic asymmetry. Here we present a simple example of one such model. The model is designed to express several of the feedbacks illustrated in Figure 4(a): reduced insolation on equator-facing slopes reduces ET, which increases soil moisture, decreases plant water stress, and promotes plant biomass production, which in turn retards the efficiency of erosion by runoff. The model also explores two potential relations between biomass and the efficiency of downslope soil creep. Note that these represent only a subset of the potential feedbacks, and some of the quantitative relations involved are speculative. The purpose here is to illustrate, first, that a relatively simple mechanistic model can indeed reproduce the first-order observed asymmetry, and second, that such mechanistic models provide a means of comparing different feedbacks and quantifying their impacts on topography, soil thickness, and other factors.

We consider a semiarid rainfall regime, with a dominant cover of grass vegetation, as hillslope asymmetry is usually more pronounced in water-limited conditions. The peak biomass on the ground surface in a growing season, Annual Net Above-ground Primary Productivity (ANPP) [g/m^2], is used in the model to represent the generation of biomass on topography. Based on plot-scale data compiled from experimental grassland sites in the USA from the literature, Webb *et al.* (1978) develop an empirical equation that relates ANPP to annual evapotranspiration (AET) [mm/y]. Their equation did not consider the role of plant water stress on growth. Depending on differences in seasonal rainfall regime, local slope, and aspect, plant water stress may show variability from site to site under a similar AET. We conceptualize the role of plant water stress on ANPP using the static water stress concept of Porporato *et al.* (2001):

$$B = B_1(1 - \xi) \tag{A1}$$

$$B_1 = 496 - 666\exp(-0.00025AET) \tag{A2}$$

$$\xi = \left(\frac{s^* - \langle s \rangle}{s^* - s_{wp}}\right)^p \tag{A3}$$

where B is biomass expressed as ANPP [g/m^2] and modified by water stress, ξ [0–1], B_1 is the maximum (stress-free) ANPP as given by the equation of Webb *et al.* (1978) (Equation (2)), $\langle s \rangle$ is the mean-annual root-zone soil moisture represented in terms of degree of saturation [0–1], s_w and s^* are soil moisture levels corresponding to soil water potentials at wilting point and incipient stomata closure, respectively, and p is a parameter ($p > 1$) (Porporato *et al.*, 2001).

Terrain is represented as a grid of elevation values, and B is calculated at each grid cell of the model using spatially varying inputs of $\langle s \rangle$ and AET. We used the minimalistic soil moisture dynamics model of Porporato *et al.* (2004) to obtain local $\langle s \rangle$ and AET. The model is driven by depth and arrival statistics of storms and a spatially distributed field of potential evapotranspiration, while omitting lateral transport of soil moisture. Defining an effective relative soil moisture term, $x = (s - s_w)/(s_{fc} - s_w)$, and using Poisson arrival of storms with frequency λ [1/day] and a mean storm depth α [mm], the temporal mean of x at each model element is calculated by (Porporato *et al.*, 2004):

$$<x>=\frac{1}{\eta\gamma}\left(\lambda-\frac{\eta\gamma^{\lambda/\eta}}{\Gamma(\lambda/\eta)-\Gamma(\lambda/\eta,\gamma)}e^{-\gamma}\right) \quad \text{(A4)}$$

$$\gamma=\frac{w_o}{\alpha},\ \ \eta=\frac{ET_{\max}}{w_o},\qquad w_o=(s_{fc}-s_w)nZ_r \quad \text{(A5)}$$

where, n is soil porosity, Z_r is depth of ecohydrologically active root zone [mm], w_o is maximum plant available soil water storage [mm], $ET_{\max}$ is a seasonally average value of potential evapotranspiration [mm/d] at each cell of the modeled domain, and $\Gamma()$ and $\Gamma(,)$ are complete and incomplete gamma functions, respectively. From this model, AET for the duration of a season is:

$$AET=<x>\,ET_{\max}T_{season} \quad \text{(A6)}$$

$$ET_{\max}=ET_{\max-F}f_{Rc} \quad \text{(A7)}$$

In the model we assumed no seasonality and therefore used T_{season} = 365 days. The model represents the connection between aspect, insolation, soil moisture, and vegetation as follows. An annually averaged value of $ET_{\max}$ is used which was estimated by scaling $ET_{\max}$ on flat surface $ET_{\text{max-}F}$ with the ratio of clear-sky radiation on an inclined surface to clear-sky radiation on flat surface, f_{Rc}. Thus, ET varies with aspect, and this variation in turn influences biomass dynamics.

Equations (A1)–(A7) were solved numerically on a gridded representation of a hypothetical evolving topography. The numerical model was constructed using the Landlab Toolkit (Hobley *et al.*, 2017). For a given latitude we calculated daily clear-sky radiation incident on flat surface, $R_{c\text{-}F}$ [W/m^2], using the Landlab Radiation component, which follows the ASCE-EWRI (2005) formulations. $ET_{\text{max-F}}$ is approximated as the water equivalent of 50% of the mean daily R_c in a year (Irmak *et al.*, 2008). The practical assumption behind this is that 50% of the energy is lost during the complex radiation and energy balance process that involves reflection from the surface, and heat losses to the air and the ground. The Landlab radiation component approximates f_{Rc} as the ratio of the cosine of solar angle of incidence on sloped and flat surfaces (Bras, 1990).

Evolution of soil-mantled landscapes is modeled using a linear hillslope diffusion rule and a detachment-limited fluvial incision rule (Howard, 1994), modified to incorporate the impeding effect of plant biomass on soil erodibility:

$$\frac{\partial z}{\partial t}=U-\nabla\cdot(k_dS)-k_f\exp\left(-v_f\frac{B}{B_{\max}}\right)A^MS^N \quad \text{(A8)}$$

where z is the land surface elevation [m], U is uplift rate [m/y], k_d is hillslope diffusivity coefficient [m^2/y], S is local slope, k_f is coefficient for bare soil erodibility by runoff [m$^{(1-2M)}$/y], v_f is empirical vegetation impediment factor for runoff erosion, $B_{\max}$ is the amount of biomass under which mean-annual incision rate by runoff can be neglected, A is the upslope contributing area [m^2]; and M and N are parameters whose ratio is kept to 0.5 (Tucker and Whipple, 2002). While the proposed exponential decay model of erodibility due to biomass is consistent with the concept of shear stress partitioning on surface vegetation (Le Bouteiller and Venditti, 2015; Yetemen *et al.*, 2015a), here we used it as a factor to obtain a desired ratio of erodibility between north- and south-facing hillslopes.

We ran three model simulations on a raster model of 120 by 100 nodes with 15 m spacing. The initial domain was flat, with small spatially uncorrelated perturbations added to stimulate drainage network formation. The east side of the domain is fixed as an open boundary while other sides are set as closed boundaries. Model parameters reported in Table I are selected to represent a semiarid grassland site located at 34°N, having a mean-annual precipitation of 400 mm and a soil texture of loamy sand. The empirical vegetation impediment parameter

Table A1. Parameters used in the ecogeomorphic simulations

Soil and vegetation	Climate	Landscape evolution
s_{fc} = 0.52[1]	α = 0.5 cm	U=0.0003 m/y
s_w = 0.11[1]	λ = 0.22 1/d	k_d=0.005 m^2/y – 0.01 m^2/y
s^*= 0.31[1]	$ET_{\text{max-F}}$=4.6 mm/d	k_f=0.0001 m$^{(1-2M)}$/y
n = 0.42[1]		v_f= 2.75
Zr = 40 cm		M=1, N=0.5

[1]Parameters for loamy sand soil. Laio *et al.* (2001)

used in the incision rule, v_f, is adjusted such that runoff erodibility varies by a factor of two between high and low biomass conditions. The influence of aspect and biomass on the hillslope diffusivity coefficient may vary depending on regional climate and temperature fluctuations, which regulate freeze–thaw cycles and determine whether rainsplash or bioturbation are dominant processes. A spatially uniform hillslope diffusivity (average of the range in Table A1) is used in the first simulation. To illustrate two alternative cases of hillslope erosion, in the second simulation we linearly increased k_d from a minimum value with biomass, representing a correlation between biomass and transport efficiency arising from bioturbation. This led to higher k_d on north-facing slopes (NFS). In the third model experiment we linearly decreased k_d with biomass from a maximum value, representing the role of vegetation in shielding the soil from rainsplash. This resulted in higher k_d on south-facing slopes (SFS). These linear models are given as follows:

$$\text{Linear increase k}_\text{d}\text{model}: k_d(B)=k_{d\min}+(k_{d\max}-k_{d\min})\frac{B-B_1}{B_2-B_1} \quad \text{(A9)}$$

$$\text{Linear decrease k}_\text{d}\text{model}: k_d(B)=k_{d\max}+(k_{d\min}-k_{d\max})\frac{B-B_1}{B_2-B_1} \quad \text{(A10)}$$

where $k_{d\min}$ and $k_{d\max}$ are selected minimum and maximum diffusivity, and B_1 and B_2 are parameters ($B_2 > B_1$). To scale k_d exactly between its limits, we used B_1 and B_2 as the smallest and largest modeled biomass values in a landscape in modeled equilibrium. In all cases k_d only varied by a factor of two, $k_{d\max} = 2\,k_{d\min}$. Varying both hillslope diffusivity and runoff erodibility by 100% simplifies the interpretation of model results.

All simulations were run for 1000 kyr. Landscapes attained a dynamic equilibrium after ~700 kyr. Modeled fields of elevation (Z), local slope (S), radiation ratio (f_{Rc}), biomass (B), and the relationship between local slope and upslope contributing area are plotted in Figure 5. Mean elevations of the modeled landscapes and their hillslope asymmetry indices ($HA_{\text{N-S}}$) are 49.8 m (0.12), 47 m (0.13), and 52 m (0.11), reported in the same respective order as in Figure 5. Modeled $HA_{\text{N-S}}$ values are consistent with semiarid regions of North America (Poulos *et al.*, 2012; Yetemen et al., 2015a, 2015b). In all cases NFS have up to 50% higher biomass production than SFS as a result of lower f_{Rc}, which leads to a lower plant water stress. More dendritic channel networks developed in the first and second scenarios. Effective fluvial incision with lower hillslope diffusion on low-biomass SFS and bioturbation enhancement to hillslope diffusivity on high-biomass NFS provide the highest $HA_{\text{N-S}}$ and the lowest mean elevation. Higher hillslope diffusion on SFS (i.e. rainsplash effect) impedes northward valley growth by filling-in channels incised by effective fluvial processes under low biomass cover resulting in the lowest $HA_{\text{N-S}}$ and highest mean elevation. The slope–area data reveal the steeper development of SFS which occupy 17%, 13%, and 19% more landscape area than NFS, respectively in Figure 5. The higher-diffusivity-NFS simulation gives steeper slopes on both north and south aspects compared with the

other two scenarios. Results suggest that contrasting effect of biomass on fluvial and diffusive processes enhance the development of valley asymmetry and create steeper slopes.

Appendix B: Numerical modeling of short-timescale CZ processes using TIMS

TIMS represents solar radiation transfer through the vegetation canopy over flat surfaces using a two-stream approximation scheme, which accounts for multiple scattering of light by the canopy and ground in two mainstreams (upward and downward) over two wave bands (visible and near-infrared) (Dickinson, 1983). Photosynthetic active energy (PAR) is then computed as the insolation absorbed by sunlit and shaded leaves over the visible band. It also considers the effects of between- and within-vegetation gaps that are controlled by the canopy structure, tree density, leaf density (LAI), and solar zenith angle (Niu and Yang, 2004). Most recently, we implemented a radiation correction scheme (RADCOR) accounting for the effects of topographic shading and scattering into TIMS. For each time step and at each pixel, RADCOR first checks if the pixel is self-shaded by comparing solar elevation angle (SEA) with the local slope and aspect angles. In turn, shading by neighboring pixels is computed by comparing SEA with the elevation angle of the lines connecting the pixel to other nearby pixels in the azimuth direction (Aguilar *et al.*, 2010). Then RADCOR corrects the diffuse radiation by considering the sheltering effects of neighboring pixels, which is evaluated by sky view factor under the isotropic sky assumption. Finally, diffuse radiation reflected from neighboring pixels is added to the pixel using isotropic conception proposed by Dozier and Frew (1990).

Marshall Gulch ranges from 2200 m to 2700 m in elevation. The climate of Marshall Gulch is subhumid with an average annual precipitation of 670 mm and annual runoff of 230 mm. The annual mean surface air temperature is 9.2°C. TIMS are integrated at 10 m resolution for 8 years from 2007 to 2014 driven by the near surface atmospheric forcing data observed at the Bigelow flux tower site, which is situated 3.5 km away from the Marshall Gulch at a similar height (2583 m). The forcing data include downward shortwave and longwave radiation, air temperature, humidity, and pressure, and wind speed, while the precipitation data are from the rain gauges within the catchment. The total downward shortwave radiation is split into direct and diffuse radiation fluxes following De Jong (1980).

The shading effects vary systematically with the azimuth angle (or aspect) of the slopes (Figure B1). The solar radiation absorbed by the polar-facing hillslopes drops by up to 60%, while that by the equator-facing hillslopes does not show much changes relative to a flat surface (FLAT). However, only a small portion of the reduced net radiation is partitioned into latent heat (or ET; Figure 7(b)) while much more is partitioned into sensible heat (Figure 7(c)). Accordingly, both above- and below-ground biomass and fluxes are affected through changes in light limitation and associated changes in soil water availability and soil temperature. Changes in LAI over the pole-facing areas are mostly scattered, reflecting the combined effect of changes in light and water limitations.

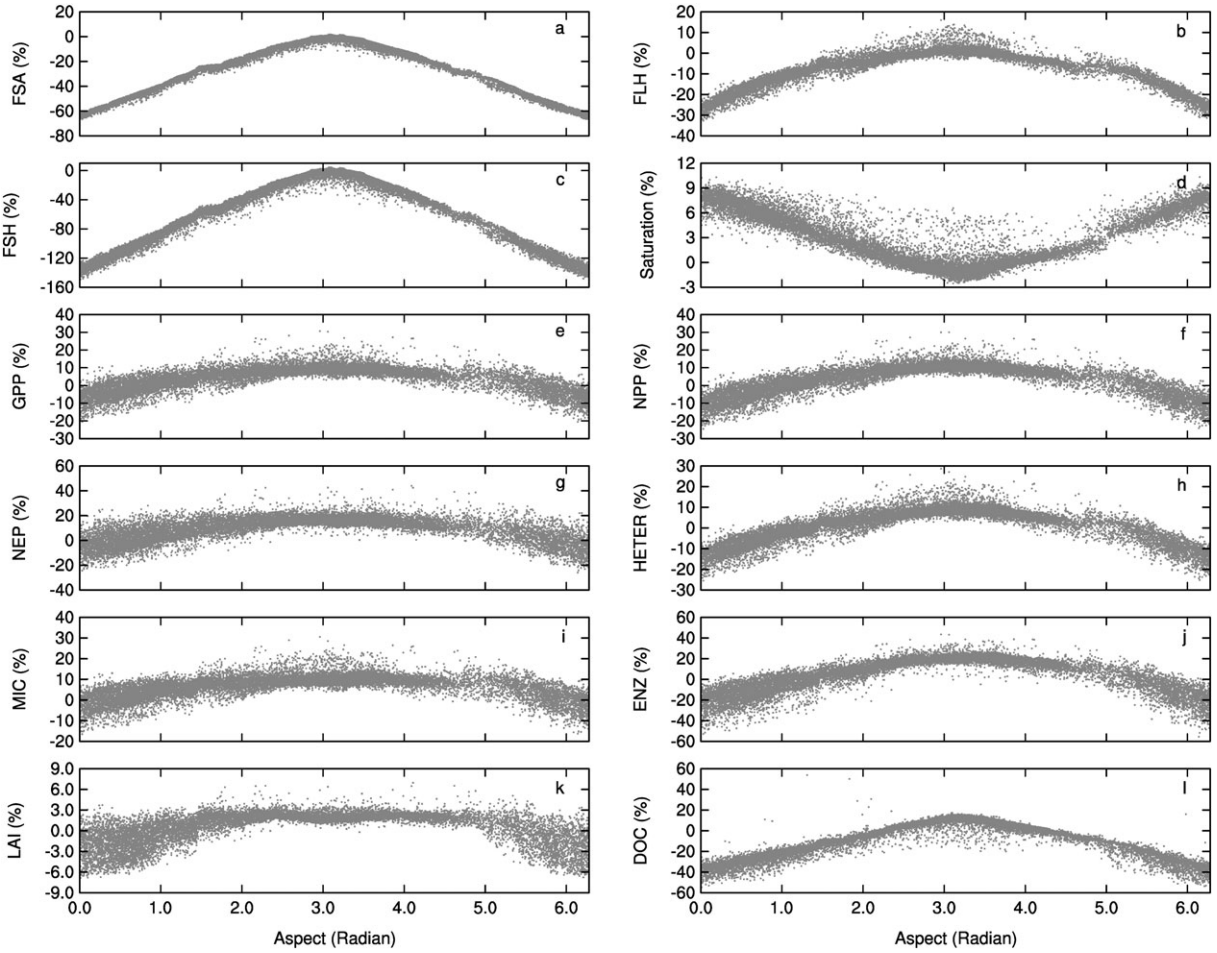

Figure B1. TIMS modeled relative change (%) of RADCOR to FLAT with slope aspect angle (in radians). (a) Net solar radiation; (b) latent heat; (c) sensible heat; (d) soil water saturation (e) GPP; (f) net primary productivity; (g) NEP; (h) microbial respiration; (i) microbial biomass; (j) enzyme; (k) LAI; and (l) dissolved organic carbon (DOC).